

Special Section:

Uncovering the hidden links between dynamics, chemical, biogeochemical and biological processes under the changing Arctic

Key Points:

- Dissolved rare earth elements (REEs) and neodymium (Nd) isotopes are constant in the deep Arctic Ocean and similar in the Eurasian and Canadian Basins
- Release of REEs from particles is limited due to the dominance of lithogenic over biogenic particles
- Dissolved REE concentrations and Nd isotopes are not significantly affected by hydrothermal activity on Gakkel Ridge

Supporting Information:

Supporting Information may be found in the online version of this article.

Correspondence to:

R. Paffrath,
ronja.paffrath@uni-oldenburg.de

Citation:

Paffrath, R., Pahnke, K., Böning, P., Rutgers van der Loeff, M., Valk, O., Gdaniec, S., & Planquette, H. (2021). Seawater-particle interactions of rare earth elements and neodymium isotopes in the deep central Arctic Ocean. *Journal of Geophysical Research: Oceans*, 126, e2021JC017423. <https://doi.org/10.1029/2021JC017423>

Received 31 MAR 2021

Accepted 3 JUL 2021

Author Contributions:

Conceptualization: Katharina Pahnke

Funding acquisition: Katharina Pahnke

© 2021. The Authors.

This is an open access article under the terms of the [Creative Commons Attribution-NonCommercial-NoDerivs License](https://creativecommons.org/licenses/by/4.0/), which permits use and distribution in any medium, provided the original work is properly cited, the use is non-commercial and no modifications or adaptations are made.

Seawater-Particle Interactions of Rare Earth Elements and Neodymium Isotopes in the Deep Central Arctic Ocean

Ronja Paffrath¹ , Katharina Pahnke¹ , Philipp Böning¹, Michiel Rutgers van der Loeff² , Ole Valk² , Sandra Gdaniec^{3,4} , and H el ene Planquette⁵ 

¹Marine Isotope Geochemistry, Institute for Chemistry and Biology of the Marine Environment (ICBM), University of Oldenburg, Oldenburg, Germany, ²Alfred-Wegener-Institute, Helmholtz Centre for Polar and Marine Research, Bremerhaven, Germany, ³Department of Geosciences, Swedish Museum of Natural History, Stockholm, Sweden, ⁴Laboratoire des Sciences du Climat et de l'Environnement, LSCE/IPSL, CEA-CNRS-UVSQ Universit  Paris-Saclay, Gif-sur-Yvette, France, ⁵University of Brest, CNRS, IRD, Ifremer, LEMAR, Plouzan , France

Abstract In the central Arctic Ocean, dissolved rare earth element concentrations ([dREE]) and the neodymium (Nd) isotope compositions are constant throughout the deep water column (>1,000 m water depth), indicating unique conditions among the ocean basins and therefore requiring an investigation of seawater-particle interactions. Here, we present the first high-resolution particulate REE and Nd isotope data from the Arctic Ocean and discuss the possible seawater-particle processes affecting the Arctic Ocean. Our results show that particulate [REE] are on the same order of magnitude as in other ocean basins, suggesting that particle composition is the main cause for a lack of pREE release to the dissolved pool. The lithogenic fraction dominates throughout the water column while the biogenic material contribution is very small. This paucity of biogenic material results in reduced particle-seawater exchanges of REEs and Nd isotopes. Moreover, we note only slight differences in the dissolved Nd isotope composition between the Eurasian and Canadian Basins. This is due to the different source regions supplying different dissolved and particulate Nd isotope signatures to both basins. The dissolved [REE] and Nd isotope composition of Atlantic waters are modified during their flow paths through contributions from the Kara Sea, lowering the salinity and increasing [dREE] and dNd isotope compositions. Hydrothermal influence from the Gakkel Ridge on dissolved and particulate [REE] and Nd isotopes could not be detected.

Plain Language Summary The Arctic Ocean is strongly affected by climate change. Due to rising temperatures, the sea-ice is melting and the river input is increasing. This will also change the chemical composition of the Arctic Ocean and biological activity, since many trace elements added by rivers are essential for algal growth. In order to understand these changes and effects, the environmental conditions and processes need to be understood. We investigated rare earth element (REE) concentrations and Nd isotope compositions in seawater and in suspended particles in the central Arctic Ocean. The data show that the release of REEs from particles to seawater is lower in the Arctic Ocean than in other ocean basins and that this is due to the lower amount of biogenic relative to terrestrial-derived particles in the Arctic Ocean. This leads to constant dissolved REE concentrations in the Arctic water column, in contrast to increasing concentrations with depth in other oceans. We further investigated the potential modification of REEs and Nd isotopes in the hydrothermally influenced deep waters over the Gakkel Ridge. In this study, we did not find an impact of the hydrothermal activity on REEs or the Nd isotope composition.

1. Introduction

The sensitive and marked response of the Arctic to current climate warming requires a robust understanding of the natural conditions and biogeochemical processes in this area to allow for future evaluations of the impact of these changes on this unique environment (e.g., IPCC, 2014). Particularly, the nutrient and trace metal composition of the Arctic Ocean, that is, expected to change due to changes in, for example, sea ice cover, river discharge, and melting of the Arctic permafrost, are of high interest due to their high relevance for Arctic ecosystems. Through waters emerging from the Arctic Ocean through the Fram Strait, any

Investigation: Ronja Paffrath
Resources: Katharina Pahnke
Supervision: Katharina Pahnke
Visualization: Ronja Paffrath
Writing – original draft: Ronja Paffrath, Katharina Pahnke, Philipp Böning, Michiel Rutgers van der Loeff, Ole Valk, Sandra Gdaniec, H el ene Planquette
Writing – review & editing: Ronja Paffrath, Katharina Pahnke, Philipp B oning, Michiel Rutgers van der Loeff, Ole Valk, Sandra Gdaniec, H el ene Planquette

such changes will also have downstream effects on the North Atlantic and the composition of deep waters formed there.

Given their terrestrial origin and biological inactivity, rare earth elements (REEs) and neodymium (Nd) isotopes can be used to study inputs, transport and cycling of trace elements to and within the ocean. REEs in seawater show a fractionation between light REEs (LREEs) and heavy REEs (HREEs) due to their differences in complexation strength with carbonate ions from seawater (e.g., Byrne & Kim, 1990; Schijf et al., 2015). It has been reported for several oceans that dissolved REE concentrations ([dREE]) are low at the surface as a result of particle scavenging, and the dLREEs are preferentially scavenged over the dHREEs (e.g., Byrne & Kim, 1990; Sholkovitz, 1995). There are very few studies on incorporation of dREEs by plants or animals, and the processes for incorporation and possible fractionation are not well understood (e.g., Akagi & Edanami, 2017; Lagarde et al., 2020; Roberts et al., 2012).

Deeper in the water column, [dREE] increase due to REE release from particles and input from sediments/pore waters (e.g., Abbott et al., 2015; Elderfield, 1998). In addition to the vertical processes controlling [dREE] in the ocean, lateral transport of dREEs must also be considered (Basak et al., 2015; Behrens, Pahnke, Schnetger, & Brumsack, 2018; Stichel et al., 2015; Zheng et al., 2016). REEs in suspended marine particles are associated with the lithogenic and/or an authigenic fraction, where the authigenic fractions that REEs preferentially adsorb to are organic and/or Fe/Mn-oxide particles (Sholkovitz et al., 1994; Tachikawa et al., 1999).

Nd isotope ratios ($^{143}\text{Nd}/^{144}\text{Nd}$, expressed as $\epsilon_{\text{Nd}} = [({}^{143}\text{Nd}/{}^{144}\text{Nd})_{\text{sample}}/({}^{143}\text{Nd}/{}^{144}\text{Nd})_{\text{CHUR}} - 1] \times 10^4$, with CHUR: Chondritic Uniform Reservoir, Jacobsen & Wasserburg, 1980) have been used to trace water mass transport, mixing of water masses, and continental input (e.g., Behrens, Pahnke, Paffrath, et al., 2018; Lacan & Jeandel, 2001; Lambelet et al., 2016; Osborne et al., 2014). They are often used in combination with REEs to provide insight into trace element sources and particle-seawater exchange (e.g., Garcia-Solsona et al., 2014; Molina-Kescher et al., 2014; Rousseau et al., 2015).

In order to use [REE] and Nd isotopes as tracers, it is crucial to identify their sources and sinks as well as their behavior in the ocean. One important aspect is the interaction between the dissolved and particulate phase. The degradation of particles while sinking through the water column typically results in increasing [dREE] and decreasing dHREE/LREE ratios with depth as the preferentially scavenged LREE are released back to the dissolved pool (e.g., Sholkovitz et al., 1994). Dissolution of lithogenic particles can result in different Post-Archean Australian Shale (PAAS)-normalized dREE patterns in seawater that are typically flat (equal normalized concentrations for all REEs) but depend on the source material. For example, Pearce et al. (2013) showed positive dEu-anomalies (anomaly is defined as the deviation of a single element in comparison to its theoretical concentration calculated by the neighbor elements, all normalized to shale, for details see Method section), reduced dCe-anomalies and flat dREE patterns in seawater as the result of the dissolution of basaltic material. Furthermore, Grenier et al. (2013) explained a positive dEu-anomaly in subsurface, intermediate and deep-water masses in the Pacific Ocean by REE inputs due to submarine weathering of basaltic sediments deposited on the margins. Particle-seawater exchange of Nd isotopes without a significant net change in [dNd] is key to the “boundary exchange” concept (e.g., Jeandel et al., 2013; Lacan & Jeandel, 2005) and has also been suggested as a mechanism explaining suspended particles in the open ocean that typically show the same ϵ_{Nd} as surrounding seawater (e.g., Tachikawa et al., 1999; van de Flierdt et al., 2012). Similarly, a change in $d\epsilon_{\text{Nd}}$ was observed in a hydrothermal plume due to exchange with hydrothermal Fe-Mn-oxide particles (Stichel et al., 2018) and in laboratory experiments where particles were exposed to seawater (Pearce et al., 2013) despite a net removal of dNd from seawater in both studies. However, due to a lack of samples of suspended particles overall, these interactions are barely studied and pREE data for the Arctic Ocean have so far been missing.

In the Arctic Ocean, [dREE] depth profiles are very different from those observed in other ocean basins: instead of an increase with depth, the [dREE] in the Arctic Ocean below the surface, where [dREE] are extremely high, are very constant (Andersson et al., 2008; Porcelli et al., 2009; Westerlund &  ohman, 1992; Yang & Haley, 2016; Zimmermann et al., 2009). The authors of these previous studies attributed this to low particle release of REEs due to generally low suspended particle concentrations. In contrast to other ocean basins, it was suggested that there is less scavenging at the surface due to fewer particles as a result

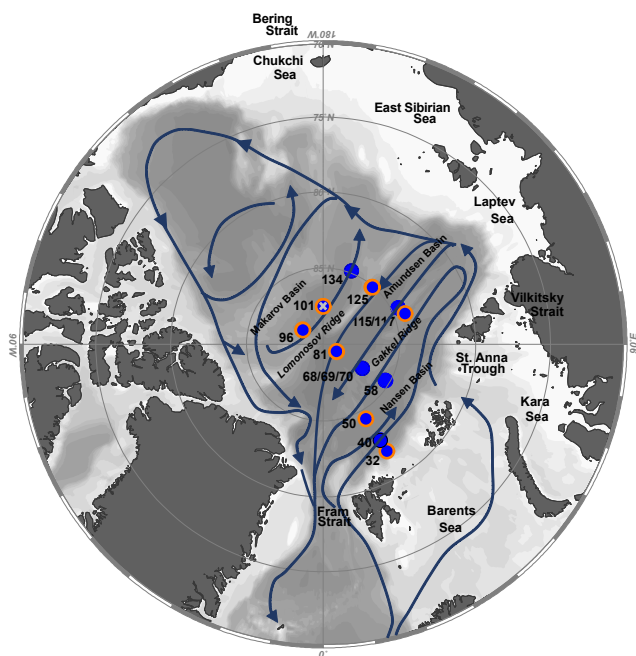


Figure 1. Map of the study area. Sampled stations of cruise PS94 are shown with blue dots for dissolved samples and orange circles for particle samples. The crossover station with USCGC Healy cruise HLY1502 is marked by a cross. Dark blue arrows show the schematic circulation of subsurface and intermediate waters after Rudels (2009). The deep-water circulation is nearly identical to the intermediate circulation. The map was produced using Ocean Data View (Schlitzer, 2018) and modified manually.

of limited biological productivity (Fernández-Méndez et al., 2015), resulting in low particle fluxes. However, direct [pREE] or pNd isotope data in combination with the dREE pool were not available from the Arctic Ocean for these studies.

In this study, we present dissolved and particulate [REE] and ϵ_{Nd} from the Atlantic water layer to the deep waters in the Arctic Ocean (water depths below 200 m) along a transect in the central Arctic Ocean through the Nansen, Amundsen, and Makarov Basins. We investigate their composition in the different water masses and their modification in the Arctic Ocean. These results allowed us to test the hypothesis, formulated by Yang and Haley (2016), that constant [dREE] with depth are explained by low particle concentrations and hence little REE release at depth.

2. Materials and Methods

2.1. Sampling and Onboard Procedures

Seawater samples were collected at 10 stations in the central Arctic Ocean during R/V Polarstern cruise PS94 (ARKXXIX/3, Tromsø-Bremerhaven, August–October 2015) as part of the European GEOTRACES section GN04. The sample locations are shown in Figure 1. Seawater was sampled from 24L-Niskin bottles using GEOTRACES protocols (Cutter et al., 2017) and directly filtered through AcroPak™ 500 Capsules with Supor® Membrane (pore size 0.8/0.2 μm) into acid-cleaned LDPE containers for Nd isotope analyses (10 L), and HDPE bottles for [REE] analyses (100 mL) using Teflon-lined Tygon® tubing. The AcroPak™ 500 cartridges were precleaned with seawater before sampling and rinsed with MQ water in between the stations. Samples for Nd isotopes were acidified with 6 N ultrapure distilled HCl to a pH of ~ 3.5 and Nd was preconcentrated using one SepPak® C18 cartridge (Waters Inc.) per 5 or 10 L sample onboard. The cartridges were preloaded with 300 mg of 2-ethylhexyl phosphate (HDEHP, Merck) using a method modified after Shabani et al. (1992) and Jeandel et al. (1998) and previously used in our lab (Behrens, Pahnke, Schnetger, & Brumsack, 2018; Fröllje et al., 2016). Samples for REE concentrations were acidified onboard to a pH < 2 using 6 N ultrapure distilled HCl. Milli Q water from the onboard system used to wash the filters was collected to obtain total procedural blanks.

Samples from stations 69 and 70 from the Gakkel Ridge were taken from the ultra-clean sampling system as described by Slagter et al. (2017) and Rijkenberg et al. (2018) and kindly provided by Michael Staubwasser (University of Cologne, Germany). For the suspended particle samples from these stations, ~ 10 L of water from the ultra-clean sampling system were filtered through 0.45 μm Supor® (polyethersulfone) filters.

Particles from all other stations were sampled using in situ pumps (McLane and Challenger Oceanic). The seawater was pumped through acid-precleaned 142 mm diameter, 0.45 μm pore size Supor® filters. Filters were dried and cut into subsamples onboard under a laminar flow hood on an acid-cleaned cutting board using tweezers and scalpels. Until further processing, they were kept at 4°C.

2.2. Digestion of Suspended Particles

The filters containing suspended particles were processed at the Alfred-Wegener-Institute in Bremerhaven (stations 50–125; Valk et al., 2018) and at the LSCE in Gif-sur-Yvette, France (station 32 and 101, Gdaniec et al., 2020) as described in Gdaniec et al. (2018). Briefly, after drying, the filters were cut using ceramic scissors, placed into closed Teflon beakers and leached with 25–30 mL of 3 M HCl in an ultrasonic bath for 5 h at 45°C. After repeated leaching, the sample solution was decanted and evaporated to <1 mL. Organic substances were dissolved through addition of 8 M HNO₃ and concentrated H₂O₂, remaining particles were separated by centrifugation and dissolved with concentrated HF. The two solutions were combined and

passed through anionic exchange columns following the protocol described in Anderson et al. (2012). Upon separation of Th and Pa, the “iron fraction” was used for further processing for Nd isotope analysis at the ICBM as described above. Prior to the column chemistry, an aliquot of 2% of the digest was removed for REE concentration analysis.

The suspended particles from stations 69 and 70 were digested with 8M HNO₃ and 1.4 M HF at 130°C, dried down and taken up in diluted HNO₃ using the method after Planquette and Sherell (2012). A fraction of this solution was used for REE concentration analysis.

2.3. Nd Isotope Analysis

In the home laboratory at the ICBM in Oldenburg, Germany, the C18 cartridges were rinsed with 5 mL of 0.01 N ultrapure distilled HCl per cartridge to remove remaining Ba. Afterward, the REEs were eluted using 35 mL ultrapure distilled 6 N HCl per cartridge. Dissolved Nd and the particulate Nd was separated from the other REEs in a two-step column chemistry (Pin & Zalduogui, 1997). The first column filled with TrisKem TRU resin (particle size 100–150 μm) was used to remove remaining HDEHP from the cartridge. In a second step, the Nd was separated from the other REEs using TrisKem LN resin (particle size 100–150 μm). The acids (HCl and HNO₃) used for these procedures were all ultrapure distilled. The Nd isotopes were analyzed using a Thermo Scientific *Neptune Plus*TM multi-collector inductively coupled plasma mass spectrometer (MC-ICP-MS) in combination with a Cetac Aridus IITM desolvating nebulizer system for sample introduction. The Nd standard JNdi-1 was measured every 2–3 samples adjusted in concentration to that of the samples. The measured ¹⁴³Nd/¹⁴⁴Nd ratios were corrected for the instrumental mass fractionation using an exponential law and ¹⁴⁶Nd/¹⁴⁴Nd = 0.7219 (O’Nions et al., 1977). If possible, a secondary mass bias correction using a linear correlation of ¹⁴³Nd/¹⁴⁴Nd and ¹⁴²Nd/¹⁴⁴Nd was applied (Vance & Thirlwall, 2002). All data were normalized to the accepted value for the JNdi-1 standard of ¹⁴³Nd/¹⁴⁴Nd = 0.512115 (Tanaka et al., 2000). Repeated measurements of JNdi-1 during the measurement sessions yielded ¹⁴³Nd/¹⁴⁴Nd ratios from 0.512058 ± 0.000011 to 0.512167 ± 0.000016 (2 SD, *n* = 190) depending on conditions during the measurement sessions over 15 months. External reproducibility based on repeat analyses of JNdi-1 were typically better than ± 0.4 ε_{Nd} units (2 SD, *n* = 4–16 per session). The measurements of 16 duplicates showed agreement within the analytical uncertainty. The lab is intercalibrated for Nd isotope measurements through analysis of GEOTRACES intercalibration samples BATS and SAFe (Behrens, Pahnke, Schnetger, & Brumsack, 2018). Additionally, two replicate samples from the Fram Strait (sample ID: PS100, station 125, 10 and 150 m, provided by G. Laukert, GEOMAR) measured at the ICBM show agreement within the analytical uncertainty to the results measured by G. Laukert at GEOMAR (Kiel, Germany) (G. Laukert, R. Paffrath, unpubl. data). Blanks were processed in the same way as the samples and spiked with a ¹⁴⁶Nd spike for Nd quantification via MC-ICP-MS. Total procedural blanks (*n* = 3) from the shipboard MQ system were <37 pg Nd, the procedural laboratory blanks were <6 pg Nd (*n* = 16), which represents <3% and <1% of the lowest sample concentration, respectively.

2.4. REE Analysis

For the determination of REE concentrations in seawater, the method described in Behrens et al. (2016) was applied. In summary, 10–20 mL of each seawater sample was spiked using a multi-element REE spike and REEs were preconcentrated and separated from the seawater matrix with the automated seaFAST pico system (Elemental Scientific Inc.) in offline mode. For REE quantification, isotope dilution ICP-MS analysis was applied, using a Thermo FinniganTM *Element* sector field inductively coupled plasma mass spectrometer and a Cetac Aridus IITM desolvating nebulizer system for sample introduction. Nitrogen supply through the Aridus IITM reduced the oxide formation to <0.03% for Ce-oxide, oxide corrections were therefore not applied. The seawater standard SAFe 3,000 m was measured repeatedly (*n* = 13) for accuracy and external reproducibility. The values ranged from 45.4 to 48.1 pmol/kg for Nd with a reproducibility of 1.8% (1 RSD), <5.1% (1 RSD) for the other REEs and 17.6% (1 RSD) for Ce and agreed well within 7% with the published average REE concentrations (Behrens et al., 2016). The blanks were spiked after the preconcentration and/or prior to the measurement to quantify the REEs. Total procedural blanks from shipboard MQ water, procedural lab blanks (2% distilled HNO₃, seaFAST preconcentration), and analytical blanks (2% distilled HNO₃) were <1.4% (<10% for Ce) of the lowest sample concentration.

The ratios of HREE/LREE as a measure of REE scavenging (strong scavenging = high HREE/LREE) were calculated as $HREE/LREE = (Er_N + Tm_N + Yb_N + Lu_N)/(La_N + Pr_N + Nd_N + Sm_N)$ (Martin et al., 2010), where subscript N indicates normalization to PAAS (Rudnick & Gao, 2003). The standard deviation of the standard SAFe 3,000 m ($n = 13$) for HREE/LREE was 2.3% (1 RSD). Furthermore, several anomalies were calculated. Anomalies display the deviation of an normalized element or element group concentration relative to its theoretical normalized concentration calculated by the neighbor elements. In this study, all anomalies are calculated based on PAAS-normalized concentrations. Values >1 indicate a positive anomaly (higher PAAS-normalized element concentrations than expected from interpolation of the neighbor elements), values <1 indicate a negative anomaly. The gadolinium (Gd)-anomaly was calculated according to Bau and Dulski (1996) as $Gd/Gd^* = Gd_N/(0.33 \cdot Sm_N + 0.67 \cdot Tb_N)$ and the standard deviation of the standard SAFe 3,000 m for Gd/Gd* was 5.3% (1 RSD). The europium (Eu)-anomaly was calculated as $Eu/Eu^* = Eu_N/(0.67 \cdot Sm_N + 0.33 \cdot Tb_N)$ with a standard deviation of SAFe 3,000 m of 4.4% (1 RSD). The MREE-anomaly was calculated after Martin et al. (2010) as $MREE/MREE^* = 2 \cdot (Gd_N + Tb_N + Dy_N)/(La_N + Pr_N + Nd_N + Tm_N + Yb_N + Lu_N)$ and the standard deviation of SAFe 3,000 m was 2.6% (1 RSD). The uncertainties of the SAFe standard for these ratios and anomalies are plotted in the figures.

For the particle samples, the digest was taken up in 2% HNO₃ and measured using a Thermo Finnigan™ *Element II* sector field ICP-MS. Europium and Gd concentrations were corrected for interferences with oxides of Ba, La, and Ce. The concentrations were determined using an internal standard (indium) and an external calibration. The particulate [REE] are provided in pmol per kg of filtered seawater. The reproducibility of BCR-2 was 2.6% (1 RSD, $n = 3$) for Nd and generally <8% (1 RSD) for all other REEs. The standard deviations for the Eu-anomaly and HREE/LREE ratios were 5.9% and 2.8% (1 RSD), respectively.

3. Results

3.1. Hydrography

All hydrographic and geochemical data are available on PANGAEA® (Paffrath et al., 2021a, 2021b). Only samples from ≥ 200 m water depth are considered, representing the water masses (Dense) Atlantic Water ((D)AW), (Dense) Arctic Atlantic Water ((D)AAW), upper Polar Deep Water (uPDW), Eurasian Basin Deep Water (EBDW), and Canadian Basin Deep Water (CBDW) according to the definitions by Rudels et al. (2012). The samples are classified using density anomalies (σ), potential temperature (θ), and salinity. This water mass classification was chosen in agreement with Laukert et al. (2017) for a better comparability of the dNd isotope composition and concentration endmembers. For an overview, samples are shown in a plot of salinity versus potential temperature in combination with their $d\epsilon_{Nd}$ signatures (Figure 2) and assigned water masses are further listed in the data set available on PANGAEA® (Paffrath et al., 2021a). Shallower samples are discussed in Paffrath, Laukert, et al. (2021) and Charette et al. (2020). The hydrographic data of the cruise can be found on PANGAEA® (Rabe et al., 2016).

Atlantic Water and (D)AAW are located at ≤ 500 m water depth and are underlain at some stations by uPDW at 1,000 and 1,400 m water depth. All samples below that depth range are either CBDW (stations 96, 101, and 134) or EBDW (all other stations).

3.2. Nd Isotope Composition

The dNd isotope composition ranges from -8.0 to -12.5 (see Figures 3 and 4). The highest variability is found in the AW with lowest ϵ_{Nd} in the Nansen Basin (stations 32, 40, and 58) and highest $d\epsilon_{Nd}$ at stations 81–125, at 200 m depth (shallowest depth presented in this study, see Figures 3 and 4). The intermediate and deep-water $d\epsilon_{Nd}$ signals are vertically and spatially invariant at $d\epsilon_{Nd} = -10.3 \pm 0.4$ (1 SD, $n = 64$), with only a slightly more positive $d\epsilon_{Nd}$ signal in the Canadian Basin (average $d\epsilon_{Nd} = -10.0 \pm 0.4$, $n = 16$) compared to the Eurasian Basins (average $d\epsilon_{Nd} = -10.4 \pm 0.4$, $n = 48$, see Figures 3 and 4). The $p\epsilon_{Nd}$ compositions of -9.0 to -12.1 show a similar range as the $d\epsilon_{Nd}$ (Figures 3 and 5). Similar to the $d\epsilon_{Nd}$ distribution, $p\epsilon_{Nd}$ shows the largest range in the upper 500 m with minor differences generally for the different water masses. There is no significant correlation between the dissolved and particulate ϵ_{Nd} ($R^2 = 0.23$, not shown).

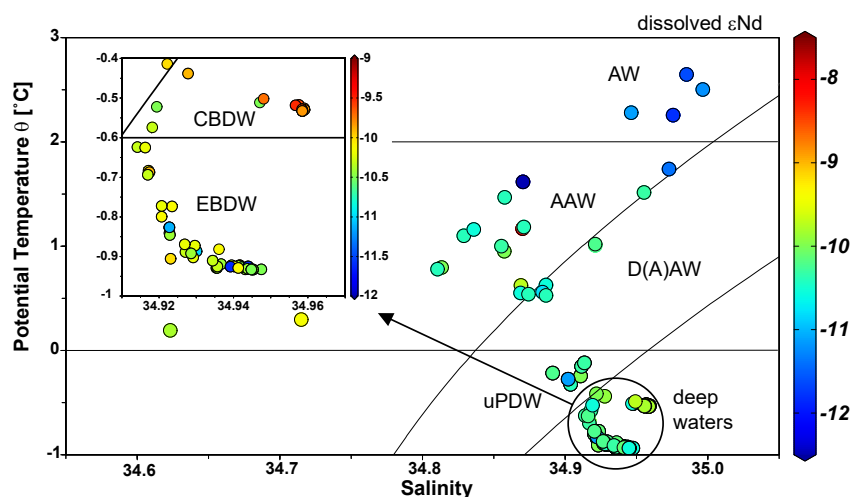


Figure 2. Salinity versus potential temperature. The colors of the dots represent the δNd isotope signatures. Water mass classifications are based on salinity, potential temperature, and density anomalies after Rudels et al. (2012). AW, Atlantic Water; AAW, Arctic Atlantic Water; D(A)AW, Dense (Arctic) Atlantic Water; uPDW, upper Polar Deep Water; EBDW, Eurasian Basin Deep Water; CBDW, Canadian Basin Deep Water. Note the different scales for the main figure and the inset. The figure was produced using Ocean Data View (Schlitzer, 2018) and modified manually.

3.3. REE Concentrations and Ratios

The [dREE] are higher in the AW than in the deeper waters (Figure 3). The [dNd] (representative for LREEs) of AW and AAW found in the central Arctic Ocean in this study range between 15.8 and 30.8 pmol/kg, and the [dEr] (representative for HREEs) range between 4.5 and 6.1 pmol/kg Er. In deeper waters ($\geq 1,000$ m water depth), the [dNd] are in the range of 13.3–17.8 pmol/kg and [dEr] from 4.0 to 5.0 pmol/kg with no significant trend with depth and no consistent differences between the stations or the basins (Figures 3 and 4). All samples show a typical PAAS-normalized seawater dREE pattern with a negative dCe-anomaly in the range of 0.1–0.3 and no systematic lateral or vertical differences. The dHREE/LREE ratios are 2.8–4.7 in AW and 3.8–4.9 in deeper waters (Figure 4c). They do not correlate with water depth and do not show a systematic spatial pattern, there is a negative correlation of dHREE/LREE versus [dNd] but not versus [dEr] (Figure S1). Dissolved Eu-anomalies are in the range of 0.9–1.3 for all water masses. The dGd-anomalies are slightly positive with 0.9–1.6 and exhibit values of up to 7 at some depths of stations 117, 125, and 134 (Figure S2).

The [REE] of suspended particles show a wide range of 0.01–4.0 pmol/kg Nd and 0.01–0.4 pmol/kg Er (Figures 3 and 5). Highest [pREE] are found at stations 32, 117, and 125 close to the slope of the Barents Sea Shelf, the Gakkel Ridge and the Lomonosov Ridge, respectively. In contrast, [pREE] are consistently low throughout the water column at stations 50, 96, and 101, with station 81 showing intermediate values. Inconsistencies in the profiles can occur due to irregular and/or inhomogeneous particle loading on the filters or incomplete dissolution during leaching. Furthermore, only a small fraction of the leachate was used for measurement of the [pREE] resulting in a low total amount of pREEs and therefore high relative standard deviations of the measured counts.

Ratios of pHREE/LREE also show a wide range from 0.2 to 6.9 with a mean of 1.4 ± 1.2 (1 SD). The pM-REE-anomalies are in the range of 0.4–1.3 (average 1.0 ± 0.2 , 1 SD) (not shown, see Paffrath et al., 2021b). The pCe-anomaly is close to 1 in most samples with a range of 0.4–2.1 and an average of 1.1 ± 0.3 , with the most negative pCe-anomalies at stations 69 and 70 (see Paffrath et al., 2021b). For all particulate ratios and anomalies there is no systematic association with water depth, basin, or dissolved or particulate [REE].

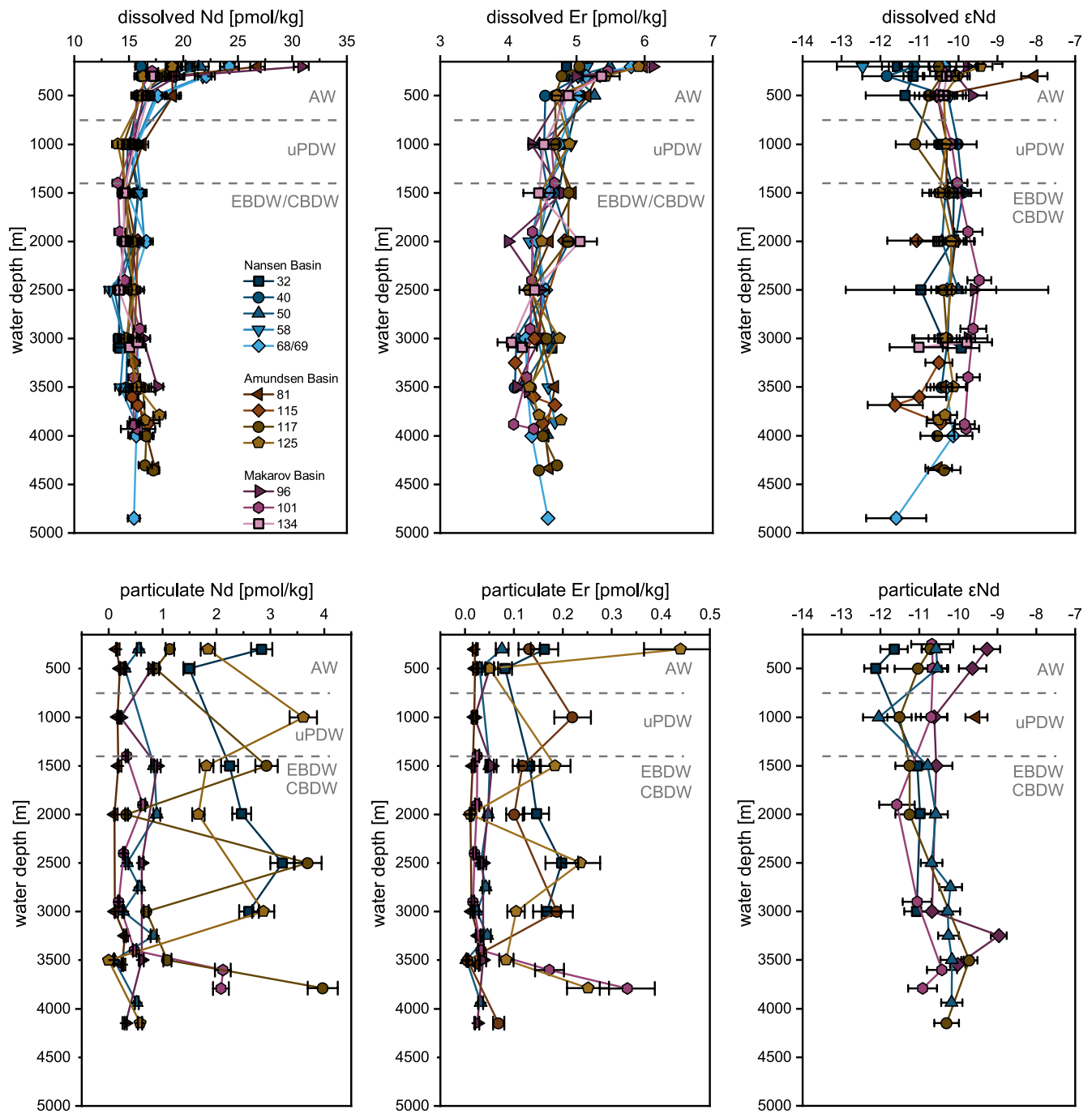


Figure 3. Profiles of dissolved (upper panel) and particulate (lower panel) neodymium (Nd) concentrations (representative for light rare earth element (REE)), erbium (Er) concentrations (representative for heavy REE), and ϵ_{Nd} .

4. Discussion

In the following, we first discuss the unique distribution of [dREE] and $d\epsilon_{Nd}$ in the central Arctic Ocean before focusing on potential particle-seawater interactions to further evaluate the dissolved seawater compositions. We then discuss the potential hydrothermal influence on seawater [dREE] and $d\epsilon_{Nd}$ and the observed exceptionally high dGd-anomalies in deep waters at some of the stations.

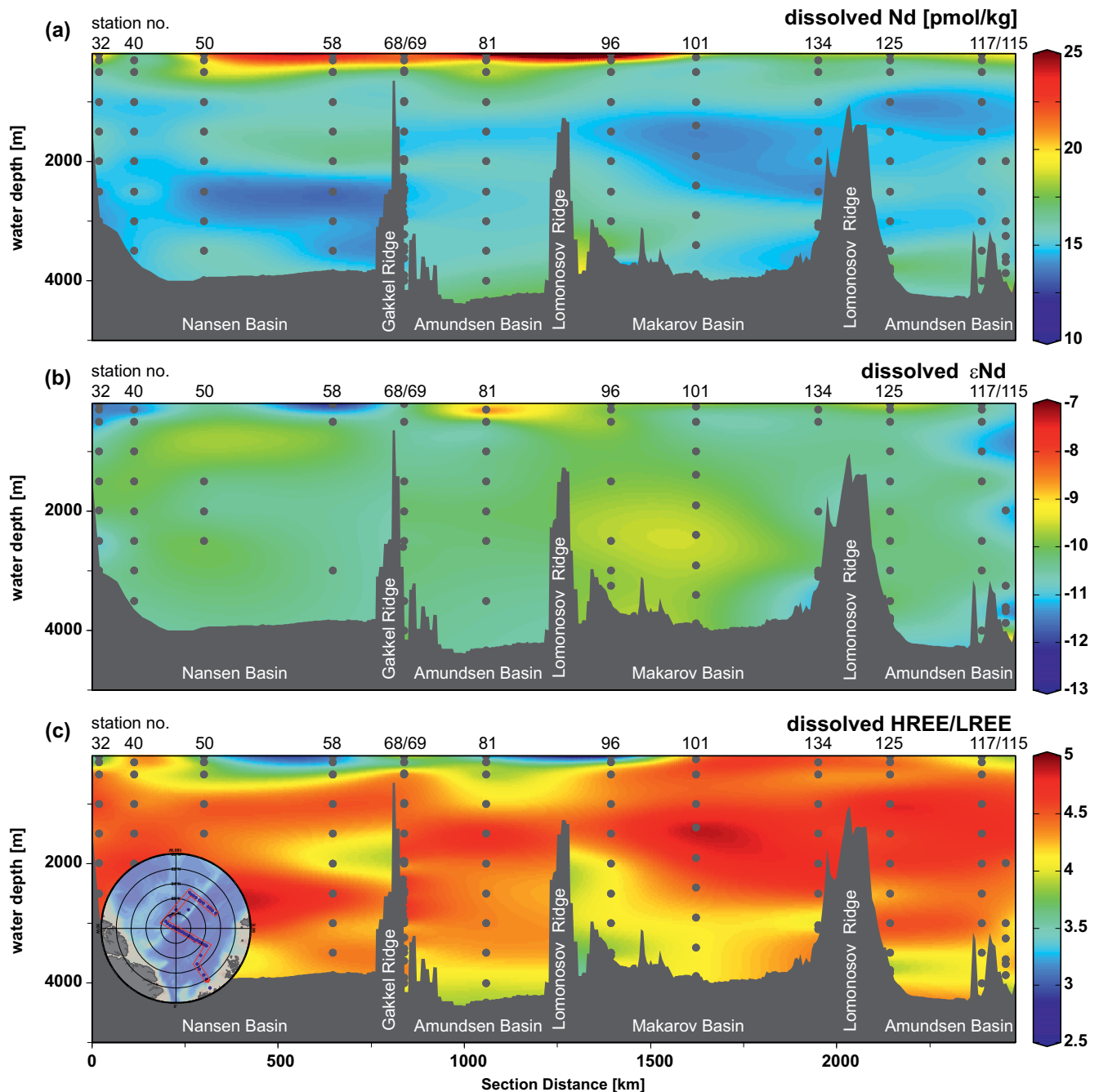


Figure 4. Sections of dissolved (a) neodymium (Nd) concentrations, (b) ϵ_{Nd} , and (c) heavy rare earth element (HREE)/light REE (LREE) ratios from 200 m water depth to the bottom. The transect is shown in the map inserted in part (c). The figure was produced using Ocean Data View (Schlitzer, 2018) and modified manually.

4.1. Evolution of $d\epsilon_{Nd}$ and [dREE] of Arctic Intermediate Waters in the Central Arctic Ocean: Atlantic and (Dense) Arctic Atlantic Water

Along its transport path from the Atlantic and throughout the Arctic Ocean, the AW ($27.7 \leq \sigma_\theta \leq 27.97$) is modified through mixing with surface or intermediate waters or admixture of shelf waters (e.g., Rudels et al., 2015). This can be seen not only in salinity and temperature but also in the dNd isotope composition and concentration: Atlantic waters entering through Fram Strait have a dNd isotope signature of $d\epsilon_{Nd} = -11.7$ (Laukert et al., 2017) is in line with the dNd isotope composition at stations 32 and 40 with an

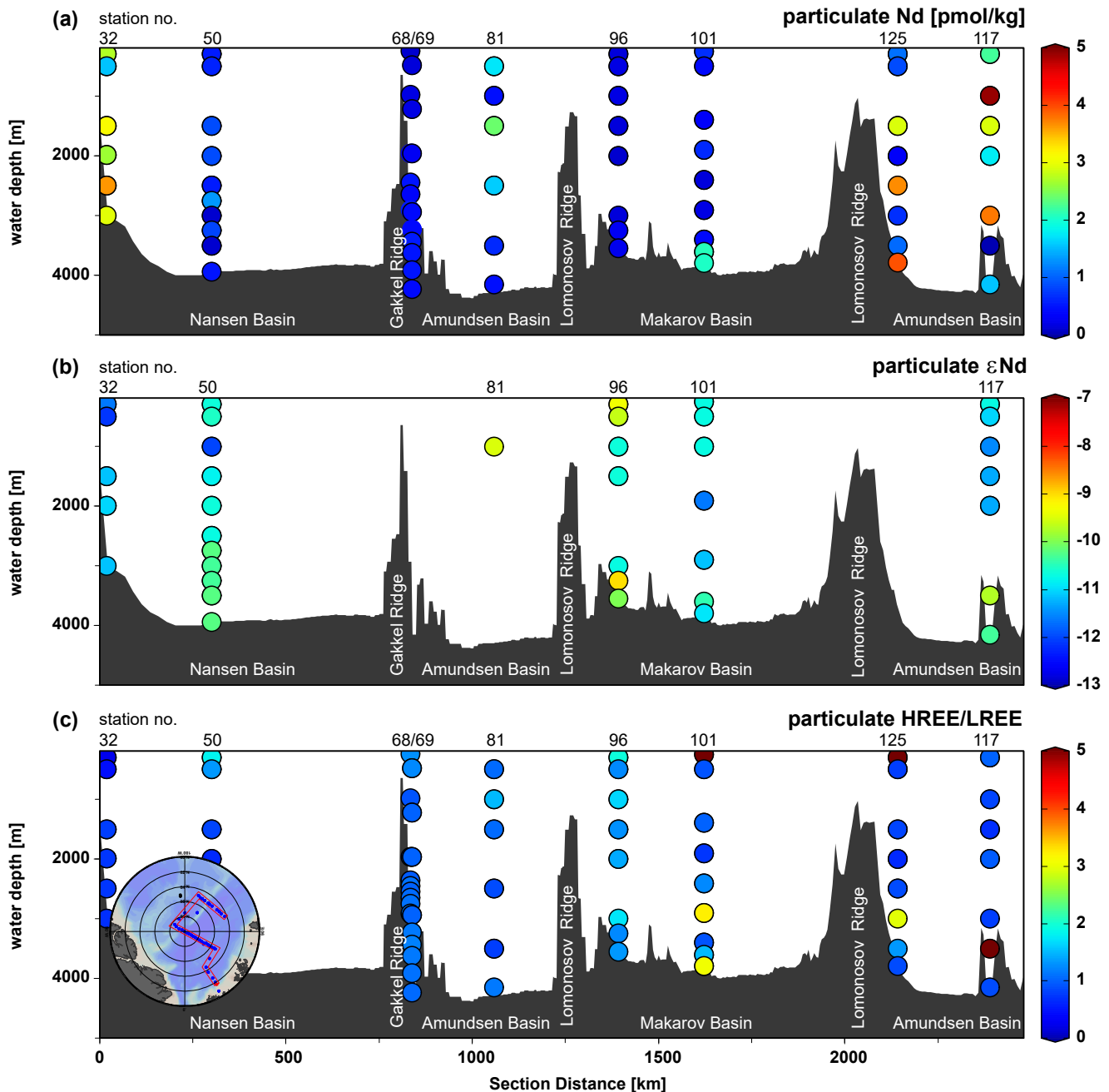


Figure 5. Sections of particulate (a) neodymium (Nd) concentrations, (b) ϵ_{Nd} and (c) heavy rare earth element (HREE)/light REE (LREE) ratios from 200 m water depth to the bottom. The transect is shown in the map inserted in part (c). The figure was produced using Ocean Data View (Schlitzer, 2018) and modified manually.

average of $d\epsilon_{Nd} = -11.4 \pm 0.3$, where pure Atlantic Water (based on potential temperature $> 2^\circ\text{C}$) is found. Further into the central Arctic Ocean, temperature and salinity decrease due to addition of river water from the Kara Sea (Laukert et al., 2017) and precipitation, and admixture of these shelf waters. This modified Atlantic Water, so-called (Dense) Arctic Atlantic Water ((D)AAW, $0 \leq \theta \leq 2^\circ\text{C}$), is seen at all other stations and shows an average of $d\epsilon_{Nd} = -10.3 \pm 0.8$, which is higher than the Atlantic Water (Figures 2 and 4). This change is consistent with admixture of Kara Sea water that is influenced by freshwater input from the Yenisei ($d\epsilon_{Nd} = -5.2$) and Ob rivers ($d\epsilon_{Nd} = -6.1$) (Laukert et al., 2017; Zimmermann et al., 2009). Similarly, the $[dNd]$ is higher in the (D)AAW ($dNd = 19.3 \pm 3.5$ pmol/kg) than in the AW ($dNd = 17.9 \pm 2.2$), consistent

with addition of river water with high [dREE] (Charette et al., 2020; Paffrath, Laukert, et al., 2021; Zimmermann et al., 2009). Addition from the Siberian shelf seas to (D)AAW has also been suggested by Liguori et al. (2020) based on heavy dissolved Si isotopes. The [dREE] are highest for samples in the transition to the overlying Polar Mixed Layer that carries the river signal and most of these samples show a low salinity in line with highest river inputs. Along the flow path, the dHREE/LREE ratios decrease in the AW and show a negative correlation with [dNd], in agreement with LREE input from the shelves.

4.2. Constant $d\epsilon_{Nd}$ and [dREE] in Eurasian and Canadian Basin Deep Waters

The deep waters of the Arctic Ocean are mainly sourced by waters of Atlantic origin (e.g., Jones et al., 1995). The only deep-water inflow is Nordic Sea Deep Water through Fram Strait with $d\epsilon_{Nd}$ of -10.0 and 16.1 pmol/kg dNd in the Fram Strait (Laukert et al., 2017). The other source for deep waters are cold, saline and dense shelf water plumes sinking down the slope of, for example, the Barents Sea Shelf (e.g., Aagaard, 1981; Middtun, 1985; Swift et al., 1983). The resulting Barents Sea Atlantic Water ($d\epsilon_{Nd} = -11.9$, 15 pmol/kg dNd, Laukert et al., 2019) flows between Franz Josef Land and Novaya Zemlya and then continues into the central Arctic Ocean via the St. Anna Trough (Rudels et al., 2012), where it can sink to intermediate or deep-water depths of equal density. The average deep-water $d\epsilon_{Nd}$ composition in the central Arctic Ocean along our transect is -10.3 ± 0.4 (with a [dNd] range of 13.3–17.8 pmol/kg Nd), which is in the range of mixing of the possible endmembers mentioned above. A difference can be seen in the Eurasian and Canadian (in this study only Makarov) Basins due to input of water masses originating from different areas and therefore showing different Nd isotope compositions: the EBDW is with $d\epsilon_{Nd} = -10.4 \pm 0.4$ less radiogenic than the CBDW ($d\epsilon_{Nd} = -9.9 \pm 0.4$). The $d\epsilon_{Nd}$ composition in the CBDW in the Makarov Basin is in line with the one from the Canadian Basin sampled in the same year (Grenier et al., 2019). While deep waters in the Eurasian Basin have $d\epsilon_{Nd}$ in the range of the deep inflow from Fram Strait and Barents Sea, the Makarov Basin deep-water $d\epsilon_{Nd}$ requires an additional radiogenic source (Figure 2). A likely radiogenic source is modified Pacific water ($d\epsilon_{Nd} = -5.5$) sinking down the slope of the Chukchi Shelf (Dahlqvist et al., 2007; Porcelli et al., 2009). Smethie et al. (2019) used ^{14}C (from the parallel US GEOTRACES cruise GN01 in 2015) to estimate the deep-water age in the Canadian Basin to be about 450 years. In order to explain this age, they suggest the age is in steady state with the renewal time of the deep waters, or that the water is not or slowly renewed, which would be in line with the theory of an overturning event about 500 years ago suggested by Macdonald et al. (1993) and confirmed by Timmermans et al. (2003). This supports the suggestion that the radiogenic $d\epsilon_{Nd}$ values in the Makarov Basin originated from the Chukchi Shelf and were preserved in the CBDW. Even though there is exchange of deep waters between the Canadian and Eurasian Basins (Timmermans et al., 2005) across the Lomonosov Ridge (1,870 m, Björk et al., 2007), the different Nd isotopic compositions are maintained in the two basins also above the sill depth. Dissolved [Nd] are on average 15.3 pmol/kg ($n = 88$) (similar for EBDW and CBDW) and thus similar to the [dNd] of inflowing AW of 16 pmol/kg dNd (Laukert et al., 2017). There is little (max. 1.5–2 pmol/kg Nd over the last 500–1,000 m water depth at some stations) to no (HREE) increase of [dREE] toward the seafloor, suggesting only minor LREE and no HREE flux from pore fluids, in contrast to some sites in the Northeast Pacific, where significant REE fluxes from bottom sediments to the deep waters have been suggested (Abbott et al., 2015). At the same time, this indicates no or very little release of (previously adsorbed) REEs from particles, in agreement with previous observations in the Canadian Basin (Yang & Haley, 2016). The residence times of the dREEs in deep waters of the Arctic Ocean were calculated to be similar to the age of the waters (Yang & Haley, 2016), consistent with the vertically and spatially homogenous [dREE] at depth. As no significant increase of REEs is observed with water depth, the [dREE] are probably a result of the mixing of their source waters. However, a quantitative assessment of the conservative behavior of REEs in the deep Arctic Ocean is strongly hampered by the lack of information on the shelf water constituents contributing to the deep-water masses in the Arctic Ocean. Deep water is formed on the Arctic shelves through surface cooling and brine rejection during sea ice formation and little is known about the hydrographic parameters, [dREE] and $d\epsilon_{Nd}$ incorporated into these waters and their seasonal and interannual and also spatial variability. Defining the deep-water endmembers to separate conservative from non-conservative behavior of REEs is therefore not possible.

4.3. Interaction Between Particulate and Dissolved REEs

The [dNd] in Arctic deep waters (>1,500 or 2,000 m; in the range of 13.3–17.8 pmol/kg Nd), are lower than in the deep waters of most other ocean basins, where [dNd] increase on average to 29 pmol/kg dNd (Atlantic) or 37 pmol/kg dNd (Pacific) below 4,000 m water depth (e.g., van de Flierdt et al., 2016 and references therein). This is in line with a lack of inflowing bottom waters with high [dREE] into the Arctic Ocean and suggests little to no addition of REEs to Arctic seawater through release from particles falling through the water column, resuspended from the ocean floor, or through diffusive porewater flux into the water column. Constant [dREE] are in line with previous studies in the Arctic Ocean, that explained the lack of a vertical increase in [dREE] with low particle concentrations due to low primary production and a lack of transfer from the surface to the deep waters (Yang & Haley, 2016). With the first [pREE] at hand, we are now able to test this hypothesis.

The vertical exchange of water in the Arctic Ocean is strongly limited due to stratification of the upper water column as a result of high river discharge, seasonal meltwater supply and seawater inflow at depth (Rudels, 2009). Hence, it was suggested that particles introduced to surface waters by river input or biological production are removed by surface advection (Yang & Haley, 2016) and possibly recycled/remineralized in the mixed layer, minimizing export to the deeper water column. Our new [pREE] data, however, show pREEs are still present in the deeper water column and that the pREE concentration range is similar to that at several locations in the Atlantic Ocean, for which [pREE] data exist (e.g., Garcia-Solsona et al., 2014; Lagarde et al., 2020; Sholkovitz et al., 1994; Tachikawa et al., 1999; van de Flierdt et al., 2012). The pREE concentration range in this study over the entire water column at the open ocean stations (stations 50–101) is from 0.1 to 0.9 pmol/kg Nd. At stations 32, 117, and 125, the [pREE] are partly even higher (up to 4.0 pmol/kg). These stations are close to the slope of the Barents Shelf, the Gakkel Ridge or the Lomonosov Ridge, respectively, and could therefore be influenced by lateral particle addition. The concentration range of pREEs for the open ocean stations is comparable to the ranges found in the Sargasso Sea (0.1–0.8 pmol/kg Nd, down to 2,000 m, Sholkovitz et al., 1994; 0.2–0.4 pmol/kg Nd, 30 and 2,000 m, van de Flierdt et al., 2012). In the Southeast Atlantic, Garcia-Solsona et al. (2014) reported [pNd] of 0.2–0.8 pmol/kg, with sharp increases to up to 19 pmol/kg near the bottom (15–180 m above the seafloor). Highest [pREE] are found in eutrophic areas with 0.7–10 pmol/kg pNd compared to oligotrophic areas with 0.1–0.7 pmol/kg pNd in the tropical northeastern Atlantic (Tachikawa et al., 1999). Recently, Lagarde et al. (2020) reported [pNd] in the range of 0.15–6.08 pmol/kg in the North Atlantic (Figure 6a). Leaching or digestion methods vary in these studies, which limits the comparability, but overall it suggests that the [pREE] in these areas are of the same order of magnitude as those in the central Arctic Ocean despite previous suggestions of very low particle fluxes in the Arctic Ocean (Yang & Haley, 2016). Furthermore, we do not find evidence for enhanced REE scavenging at the surface (e.g., high dHREE/LREE ratios or low [dREE], Paffrath, Laukert, et al., 2021), which may be due to low concentrations of biogenic particles suggested by other studies (e.g., Liguori et al., 2020). These findings do not exclude particle removal by surface advection, but processes other than a lack of particles must be responsible for the uniform [dREE], dREE ratios, and $d\epsilon_{Nd}$ in the deep Arctic Ocean. As the [pREE] are in the same range as in other oceans (Figure 6a), we discuss reasons for the different seawater-particle processes in the Arctic Ocean compared to other oceans in the following.

One aspect that may explain the different behavior of particles in the Arctic Ocean compared to other ocean basins may be the relative importance of authigenic and lithogenic associated REEs. The relative proportions of authigenic and lithogenic REEs can be calculated using particulate ^{232}Th or Al concentrations, as presented, for example, in Garcia-Solsona et al. (2014) and Tachikawa et al. (1997) with continental crust concentrations from Rudnick and Gao (2003). Particulate ^{232}Th and Al serve as conservative tracers of the lithogenic fraction. If available, ^{232}Th is preferred to Al as Al can also have a non-crustal source (Dymond et al., 1997). The ^{232}Th -based calculated lithogenic fractions exceeding 100% only at station 50 could also be due to an excess of ^{232}Th in the particles caused by ^{232}Th in the authigenic fraction (Hayes et al., 2015; Lagarde et al., 2020), but the effect is smaller for ^{232}Th than for Al. Therefore, we used particulate ^{232}Th concentrations from Valk et al. (2018) and Gdaniec et al. (2020) (same cruise as this study) for the calculation of the lithogenic REE fraction. At most stations, the lithogenic [Nd] are constant throughout the water column (Figure 7a), whereas the authigenic fractions show a larger range from 0 to 3.5 pmol/kg pNd (see Paffrath et al., 2021b). The relative contribution of lithogenic and authigenic fractions to the total particulate

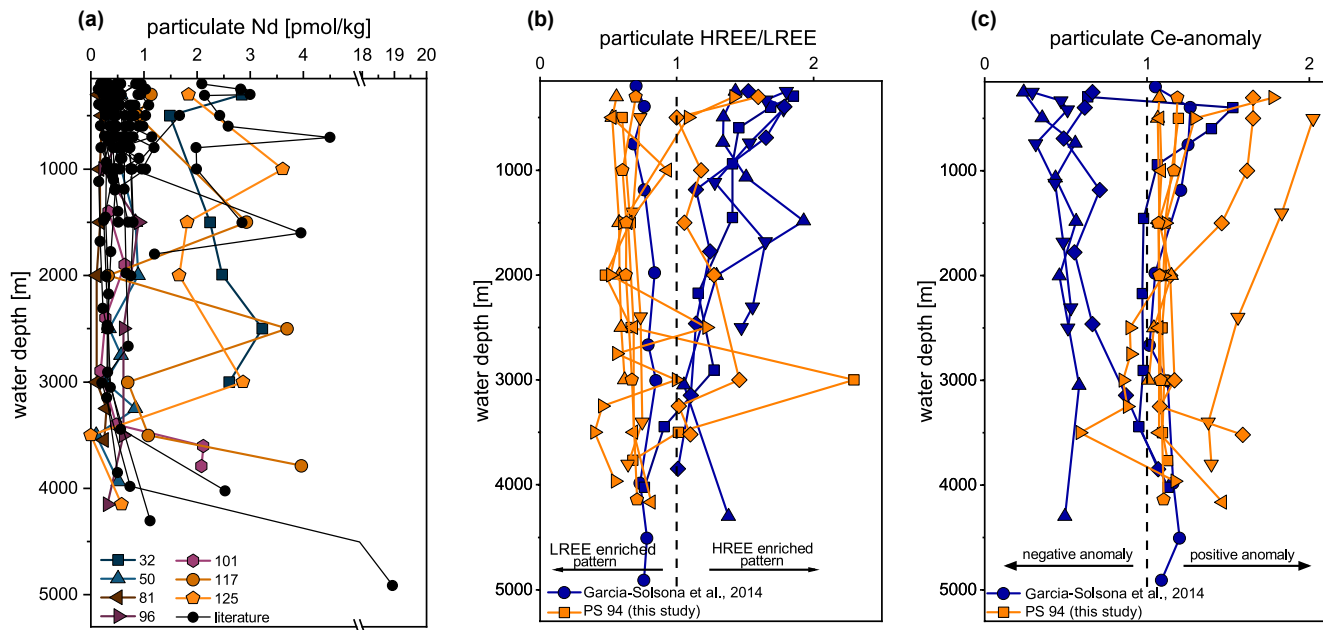


Figure 6. Comparison of particulate rare earth element (REE) data from this study and the literature. (a) Profiles of particulate neodymium (Nd) in comparison to data from Bertram and Elderfield (1993), Sholkovitz et al. (1994), Tachikawa et al. (1999), van de Flierdt et al. (2012), Garcia-Solsona et al. (2014), and Lagarde et al. (2020); (b) particulate heavy REE (HREE)/light REE (LREE) ratios and (c) particulate Ce-anomaly of this study and Garcia-Solsona et al. (2014).

concentration (presented as % lithogenic, Figure 7b) show a dominance ($\geq 50\%$) of the lithogenic fraction at most stations except a few samples from stations 50 and 125. The lack of any trends with water depth in the authigenic fraction are a result of the total [pNd] that vary with depth without showing systematic trends. In contrast to what is observed in the Arctic Ocean, most open-ocean settings show a dominance of biogenic/authigenic material in the particle composition (Lam & Marchal, 2015 and references therein), while for areas closer to the margins or with dust deposition, the lithogenic material can be the dominant contributor

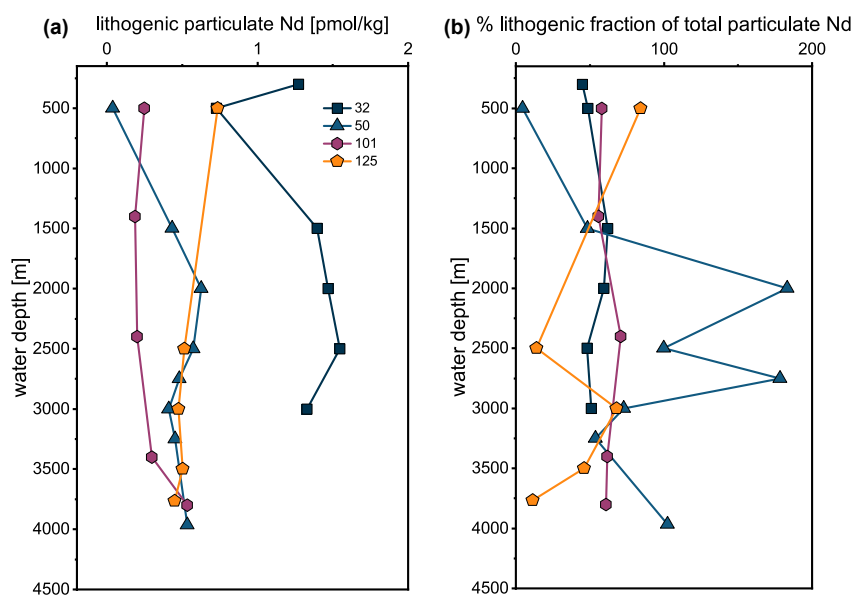


Figure 7. Lithogenic fractions of particulate neodymium (Nd). (a) Absolute lithogenic fraction of particulate Nd and (b) relative lithogenic fraction of particulate Nd. Lithogenic fractions were calculated based on ^{232}Th after Garcia-Solsona et al. (2014).

to the particle composition (Lam et al., 2015). Specifically for pREEs, authigenic particles dominate most stations in the Southeast Atlantic (Garcia-Solsona et al., 2014), whereas a dominance of the authigenic or lithogenic fraction is hard to determine in the Northeast Atlantic (Tachikawa et al., 1999) due to high errors in the calculated authigenic fraction (caused by the small difference between the measured total and the authigenic ϵ_{Nd}). In the North Atlantic, the lithogenic fraction is especially high at the margins and decreases toward the open ocean (Lagarde et al., 2020). Model tests revealed that the authigenic Nd scavenged by particles is completely remineralized in the deep ocean (Tachikawa et al., 2003), whereas the influence of lithogenic sources, for example, dust is often restricted to the surface waters (e.g., Stichel et al., 2015). Different types of particles dissolve differently with depth and also show different scavenging behavior depending on the scavenged element (Siddall et al., 2008) and the scavenger (e.g., Schijf et al., 2015).

These findings are consistent with the PAAS-normalized pREE patterns as an indicator for the lithogenic/authigenic fractionation and the seawater-particle exchange in general (Figure 8). The flat PAAS-normalized patterns of the pREEs in our study and the absence of negative pCe-anomalies point to a dominant lithogenic origin of the particles (Figures 6b, 6c and 8). In contrast, at stations in the Atlantic where authigenic phases are dominant, the bulk particle PAAS-normalized pREE patterns show a marine signature with negative pCe-anomalies and high pHREE/LREE ratios (Garcia-Solsona et al., 2014), which is not found in the particulate samples in this study (Figure 6). A dominance of lithogenic material over biogenic and authigenic material is supported by low biological productivity in the central Arctic Ocean (e.g., Fernández-Méndez et al., 2015) and comparably high lithogenic inputs from the large Siberian rivers. As the amount of authigenic particles makes up a small amount of the total particle load in the Arctic Ocean, scavenging to authigenic particles followed by a release of REEs at greater depth is limited. This results in almost constant [dREE] in deep waters in contrast to the other major oceans. This is in agreement with the dissolved Si concentrations and isotopic signatures in the deep Arctic Ocean (>200 m) that indicate a lack of biogenic Si dissolution likely caused by the overall low biogenic silica concentrations (Liguori et al., 2020). The authors suggested both low pelagic diatom production and reduced export of biogenic Si to the deeper water column due to the strong density stratification of the upper water column (Liguori et al., 2020). The minor role of the lithogenic fraction in transporting (and releasing) REEs to the deep ocean is in line with Stichel et al. (2015), who found that the influence of Saharan dust on the dNd isotope composition was limited to the very surface layer for their sampling locations in the Eastern North Atlantic.

Another parameter to describe seawater-particle interactions are the dHREE/LREE ratios. If scavenged REEs are increasingly released with depth, the dHREE/LREE ratios should decrease with increasing depth due to release of preferentially scavenged LREEs. The dHREE/LREE ratios are in a narrow range (2.8–4.9, deep waters 3.8–4.9) and only show a small dHREE/LREE decrease below 1,500 m water depth of on average 0.3 that coincides with a very small [dNd] increase (Figure S1), in line with low input of REEs at depth through release of previously scavenged REEs from particles falling through the water column. This is in contrast to other oceans, where the dHREE/LREE ratios clearly decrease and [dNd] increases with depth (e.g., Behrens, Pahnke, Paffrath, et al., 2018; Garcia-Solsona et al., 2014; Molina-Kescher et al., 2014). Lowest dHREE/LREE ratios and highest d[Nd] in the central Arctic Ocean are confined to AW at stations 32–96, likely suggesting Nd (and other REE) input from the Barents Sea shelf (Laukert et al., 2019).

An additional aspect for the constant and comparably low [dREE] in the Arctic deep water may be the age of these waters in comparison to the residence time of the dREEs. The age (isolation time) of the deep waters in the Arctic Ocean ranges from about 250 years (Eurasian Basin) to 450 years (Canadian Basin) (Schlosser et al., 1994). Yang and Haley (2016) calculated the residence time of REEs in the Canadian Basin to be 450–700 years for the Canada Basin. This estimate is comparable to the age of the deep waters. However, the authors assume that the only renewal of CBDW occurs from the Eurasian Basin over the Lomonosov Ridge. This is in contrast to the theory of Macdonald et al. (1993) (supported by Smethie et al., 2019; Timmermans et al., 2003) who suggested that the CBDW is a relic of an overturning event 500 years ago. Therefore, the residence time estimate of Yang and Haley (2016) could be taken as a minimum estimate. In general, the ages of the deep waters are young with respect to the scavenging residence time of dREEs which is 360–1900 years for Nd in the world ocean (e.g., Arsouze et al., 2009; Jeandel et al., 1995; Tachikawa et al., 1999, 2003). Calculations of the residence time are based on the inventory in the ocean and the supply or removal rate of an element. As our data suggest scavenging to be smaller in the Arctic Ocean compared

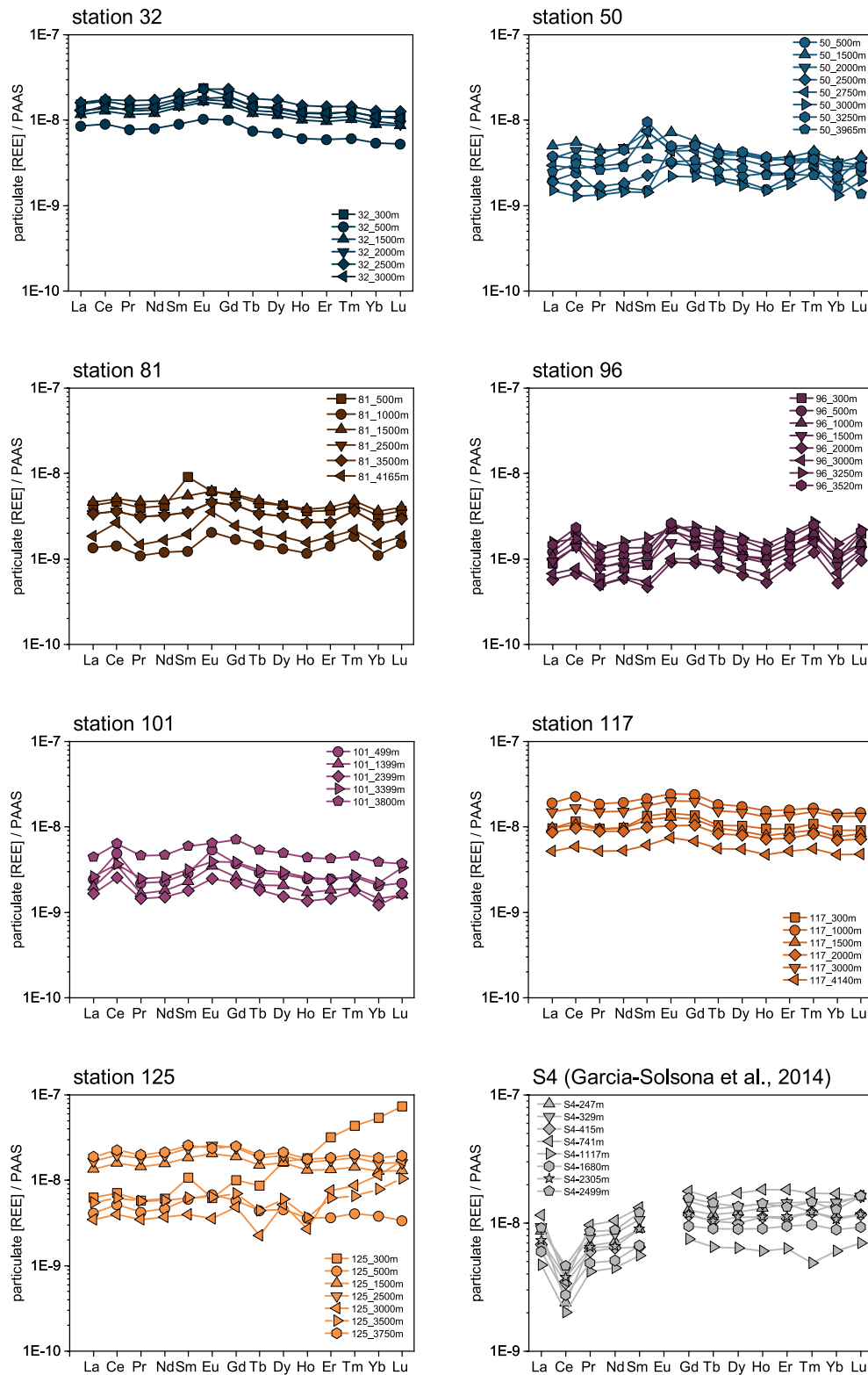


Figure 8. PAAS-normalized patterns of particulate rare earth elements (REEs) of this study showing flat or light REE and MREE enriched patterns compared to the seawater-like, heavy REE enriched particulate REE patterns reported from the southeast Atlantic (station S4) by Garcia-Solsona et al. (2014).

to other oceans, the residence time might be longer in the Arctic Ocean than the estimated global residence time. This supports the homogenous distribution in the deep waters due to largely conservative behavior of REEs.

The Nd isotopic composition of the particles is close to the dissolved one for most samples and also shows the largest range in the upper 1,000 m ($p\epsilon_{Nd} = -9.3$ to -12.1) (Figures 3–5). This could be a result of exchange of Nd between the dissolved and particulate phase or a similar ϵ_{Nd} composition of the lithogenic source and the seawater. For the authigenic fraction, a similar Nd isotope signature as the dissolved pool can be expected. A large particle source to the central Arctic Ocean are the rivers Yenisei, Ob and Lena with ϵ_{Nd} values of the riverbed sediments of -6.4 , -8.2 , and -14.8 , respectively (Schmitt, 2007). Other possible lithogenic sources, for example, from the shelves, are not characterized for Nd isotope composition. With the given sources, we cannot distinguish if the pNd isotope composition is caused by mixing of the possible lithogenic sources or by exchange with the dissolved pool or a combination of both.

To summarize, [pREE] in the Arctic Ocean are similar to those in other oceans. In contrast, there is no pronounced increase in [dREE] with depth. We suggest that this is due to the dominant lithogenic origin of the particles, whereas in other areas, for example, in the southeast Atlantic at open ocean stations, authigenic particles dominate (Garcia-Solsona et al., 2014), releasing REEs previously scavenged in the upper water column. Furthermore, the age of the deep waters is shorter or similar to the residence time of the REEs, contributing to the homogenous dREE distributions. Exchange processes among the dissolved and particulate phase can possibly alter the Nd isotopic composition, but this study cannot provide evidence due to the variety of Nd isotope compositions of the possible sources.

4.4. Hydrothermal Influence of the Gakkel Ridge Plume on dREEs and $d\epsilon_{Nd}$

Hydrothermal fluids are strongly enriched in [REE] in comparison to seawater, with a strong positive Eu-anomaly (Mitra et al., 1994). Upon mixing with seawater, Fe-Mn-oxyhydroxides precipitate and scavenge REEs, not only effectively removing the vent fluid REEs, but also leading to a depletion of seawater REEs in the hydrothermal plume (e.g., Chavagnac et al., 2018; German et al., 1990; Klinkhammer et al., 1983; Mitra et al., 1994; Stichel et al., 2018).

More recently, some studies showed that hydrothermal influence can alter the Nd isotope composition and/or concentration of seawater: for example, Jeandel (1993) found a change in the dNd isotope signature toward more radiogenic values in the vicinity of the East Pacific Rise without a change in [REE] or REE shale-normalized pattern (one sample). Similarly, Stichel et al. (2018) showed that the seawater Nd isotope signal in the plume of the TAG hydrothermal vent in the North Atlantic is shifted by up to 0.7 ϵ_{Nd} units to more radiogenic values. Additionally, these authors reported removal of dNd (1.8 pmol/kg), increased dEu-anomalies, and increased dHREE/LREE ratios within the plume relative to over- and underlying seawater and adjacent stations.

At the ultraslow spreading Gakkel Ridge, various active venting sites were found (Edmonds et al., 2003; Michael et al., 2003) defying previous assumptions that hydrothermal venting would be extremely low. Cruise PS94 transected the Gakkel Ridge and encountered a hydrothermal plume at station 70 around 2,500 m water depth that was marked by a positive temperature anomaly (Rabe et al., 2016) and elevated Fe and Si concentrations in the interval from 2,400 to 2,800 m (Interval 1 of Stranne et al., 2010) (Rijkenberg et al., 2018; van Ooijen et al., 2016, respectively). High dissolved Fe concentrations have also previously been reported and associated with the hydrothermal plume of the Gakkel Ridge (Klunder et al., 2012). Methane (Ellen Damm, pers. comm.) and particulate Fe and Mn concentrations (Hélène Planquette, pers. comm.) also show maxima at the plume depth. At station 68/69 at a deeper depth interval of 3,000–3,800 m (Interval 2 of Stranne et al., 2010), only a small positive or no anomalies for Si (depending on the station used as “background” signal) and smaller positive anomalies of particulate Fe and Mn were observed (Micha Rijkenberg, Hélène Planquette, pers. comm.), whereas dissolved Fe and methane do not show anomalies (Rijkenberg et al., 2018; Ellen Damm, pers. comm.), pointing to a smaller or no hydrothermal influence. Valk et al. (2018) found a decrease in the dissolved ^{230}Th below 2,000 m at station 68 as a result of scavenging of ^{230}Th to hydrothermal particles released from steady venting. In comparison to 2007, the dissolved ^{230}Th concentrations were lower below 2,000 m across the Nansen Basin in 2015, which the authors assigned to

a scavenging event that must have occurred in that timespan and could potentially have also affected the [REE].

There is a small decrease in [dREE] at station 70 at 2,500 m water depth relative to over- and underlying water that could be related to REE scavenging by Fe-Mn-oxides. A second [dREE] decrease of the same amplitude is seen toward the seafloor at 2,900 m water depth, which could be due to REE scavenging onto resuspended particles. A hydrothermal origin of the [dNd] depletion at the plume depth, however, is not supported by dHREE/LREE ratios or dEu-anomalies, as those values do not show systematic changes outside the analytical uncertainty (Figure S3). At stations 68 and 69, [dNd] and dHREE/LREE ratios do not differ throughout the profile, only a slight positive dEu-anomaly (1.15) is found at 3,500 m at station 68 that is higher than for the samples above and below (Figure S3). This might hint at a small hydrothermal influence that has no detectable effect on the [dREE]. For the particulate fraction, a slight increase in [pNd] and Eu-anomaly may be the result of scavenging onto hydrothermal particles like Fe-Mn-oxides, but the increases are very small. The low [^{230}Th] due to enhanced hydrothermal scavenging are also seen at other stations in the Nansen Basin (Valk et al., 2018). The slightly lower [dREE] below 2,000 m water depth in the Nansen Basin (Figures 3 and 4a) are within the analytical uncertainty to concentrations in the Amundsen and Makarov Basins and can therefore not be attributed to scavenging by hydrothermal particles in the Nansen Basin. Comparison with [dNd] measured at two stations in the Nansen Basin in 2001 (Andersson et al., 2008) does not show a significant difference to the concentrations in 2015 (this study), indicating that the hydrothermal scavenging event suggested based on [^{230}Th] (Valk et al., 2018) did not affect [dREE] noticeably.

Even if the hydrothermal influence is not seen in dissolved and particulate REE concentrations and patterns, it could influence the dNd isotope composition through exchange with Fe-Mn-oxides as suggested by, for example, Stichel et al. (2018), Chavagnac et al. (2018), and Jeandel (1993). However, no shift in the dNd isotope composition toward more radiogenic values is observed at stations 68 and 70 relative to over- and underlying samples nor adjacent stations.

In summary, the [dREE] and $d\epsilon_{\text{Nd}}$ composition are not significantly influenced by hydrothermal activity at the sampled sites. In comparison to the TAG hydrothermal plume, this can be related to the slow spreading rate at Gakkel Ridge (e.g., Michael et al., 2003). At the same time, Rijkenberg et al. (2018) showed that the hydrothermally induced increase in dissolved Fe concentrations from the same cruise in 2015 was smaller than observed in 2007 (Klunder et al., 2012) and related this to the difference in sampling location. Even though the REEs have a longer residence time than, for example, Fe and therefore the effects of hydrothermal influence can accumulate over time, the hydrothermal activity was not high enough to leave a substantial imprint on [dREE] and $d\epsilon_{\text{Nd}}$ at the stations in the hydrothermal plume (68, 69, 70) or downstream in the Nansen Basin (as reported for [^{230}Th], Valk et al., 2018).

4.5. Positive dGd-Anomaly at Stations 125 and 134

At station 125 and partly 134, there is a positive dGd-anomaly of up to 7 that is correlated with elevated [dCe] (Figure S2, for station 125: $R^2 = 0.65$, p -value < 0.05). The other dREEs and other trace metals, for example, dissolved Fe (Rijkenberg et al., 2018) do not show any conspicuous features or deviations at the same stations and depths.

Positive dGd-anomalies have been reported before in marine surface and coastal waters (e.g., Kulaksiz & Bau, 2007; Paffrath et al., 2020; Pedreira et al., 2018) and river water (e.g., Bau & Dulski, 1996; Kulaksiz & Bau, 2007). They are a result of anthropogenic influence as Gd is used in contrast agents for magnetic resonance imaging since the 1980s. These contrast agents contain Gd in strong complexes that pass the wastewater treatment plants unaffected and release Gd to the rivers and the oceans (Bau & Dulski, 1996). Therefore, positive dGd-anomalies in surface samples could be expected due to large river inputs and urban areas along these rivers, but surprisingly, they are found throughout the water column at stations 125 and 134 down to 3,788 m water depth. This makes anthropogenic contamination via contrast agents unlikely as they have been used for only about 40 years and the deep waters are older than that (250–450 years; Schlosser et al., 1994). Furthermore, in surface samples with high river contributions of up to about 21%

(Charette et al., 2020; Paffrath, Laukert, et al., 2021), a positive dGd-anomaly exceeding the natural one was not observed and the rivers are therefore an unlikely source of the high [dGd].

Natural sources of the high dGd-anomalies and elevated [dCe], such as sediments or hydrothermal input, can be excluded as no selective Ce and Gd release from minerals or elevated concentrations of these elements in minerals or hydrothermal vent fluids have been reported so far and [pCe] and [pGd] at station 125 are not elevated.

Contamination of these samples in the lab during sample processing or analysis is excluded as these samples were processed two to three times at different times, but the positive dGd-anomaly and elevated [dCe] were present in every subsample analyzed. Furthermore, these samples were prepared together with other samples in one batch that do not show a positive dGd-anomaly nor elevated [dCe]. Invoking contamination during sampling is also hampered by the lack of a potential source of high Gd and Ce on board that would selectively contaminate only some of the samples, but not others.

This leaves an in situ anthropogenic contamination as the most likely cause of the observed anomalies. The input of anthropogenic Gd from contrast agents is unlikely, as discussed above, but Gd is also used in industry in shielding of nuclear reactors and improvement of the workability and of the resistance to high temperature and oxidation of iron, chromium, and related alloys (Voncken, 2016). Further applications of Gd include the usage for optical and magnetic detection, ceramics, glasses, crystal scintillators (Naumov, 2008), and magnetic coolants (Eliseeva & Bünzli, 2011). Input of Gd due to reprocessing plants is unlikely as $^{129}\text{I}/^{236}\text{U}$ ratios at the stations and depths with positive dGd-anomalies are low (Casacuberta et al., 2018). A further discussion of potential sources for the high [dGd] and [dCe] is beyond the scope of this study. Overall, due to the regional occurrence of the dGd-anomaly, an in situ anthropogenic nearby point source, maybe on the nearby Lomonosov Ridge, is suggested to cause the increased [dGd] over a large depth range.

5. Conclusions

Deep waters from the central Arctic Ocean show uniform [dREE] as a result of very little REE input from particles, despite [pREE] in the same range as in other ocean basins. Estimates of the relative lithogenic and authigenic [REE] indicate a dominance of the lithogenic fraction. We suggest that the low concentration of biogenic particles and active recycling in the surface layer suggested by other studies (e.g., Liguori et al., 2020), are responsible for the reduced release of REEs from particles in the deep waters. The dNd isotope composition is also constant in the deep central Arctic Ocean, with only slightly more radiogenic deep water in the Canadian compared to the Eurasian Basin due to additional radiogenic input most likely from the Chukchi Shelf to the Canadian Basin. Atlantic waters evolve upon their transport from Fram Strait, as contributions from the Kara Sea lower the salinity and increase the [dREE] and dNd isotope signatures. A hydrothermal plume sampled close to the Gakkel Ridge has no influence on dissolved and particulate REE concentrations, REE patterns nor the Nd isotope composition. A positive dGd-anomaly was found at two stations probably due to a nearby point source.

Acknowledgments

The authors thank the captain S. Schwarze and the chief scientist U. Schauer as well as the crew of the R/V Polarstern cruise PS94 (ARKXXIX/3). Thanks to M. Staubwasser for providing additional water samples for station 69 and 70. Furthermore, the authors acknowledge M. Schulz for laboratory assistance. The authors thank Catherine Jeandel and Robert Newton for their constructive comments that helped improving the manuscript. This project was financially supported through the Institute for Chemistry and Biology of the Marine Environment (ICBM), the Max Planck Institute for Marine Microbiology, Bremen, and the LEFE-CYBER EXPATE. Open access enabled and organized by Projekt DEAL.

Data Availability Statement

The data used in this study are available on the PANGAEA® database (www.pangaea.de) under <https://doi.org/10.1594/PANGAEA.933493> (dissolved data; Paffrath et al., 2021a) and <https://doi.org/10.1594/PANGAEA.933484> (particulate data; Paffrath et al., 2021b).

References

- Aagaard, K. (1981). On the deep circulation in the Arctic Ocean. *Deep-Sea Research Part A*, 28, 251–268. [https://doi.org/10.1016/0198-0149\(81\)90066-2](https://doi.org/10.1016/0198-0149(81)90066-2)
- Abbott, A. N., Haley, B. A., McManus, J., & Reimers, C. E. (2015). The sedimentary flux of dissolved rare earth elements to the ocean. *Geochimica et Cosmochimica Acta*, 154, 186–200. <https://doi.org/10.1016/j.gca.2015.01.010>
- Akagi, T., & Edanami, K. (2017). Sources of rare earth elements in shells and soft-tissues of bivalves from Tokyo Bay. *Marine Chemistry*, 194, 55–62. <https://doi.org/10.1016/j.marchem.2017.02.009>

- Anderson, R. F., Fleisher, M. Q., Robinson, L. F., Edwards, R. L., Hoff, J. A., Moran, S. B., et al. (2012). GEOTRACES intercalibration of ^{230}Th , ^{232}Th , ^{231}Pa , and prospects for ^{10}Be . *Limnology and Oceanography: Methods*, *10*, 179–213. <https://doi.org/10.4319/lom.2012.10.179>
- Andersson, P. S., Porcelli, D., Frank, M., Björk, G., Dahlqvist, R., & Gustafsson, Ö. (2008). Neodymium isotopes in seawater from the Barents Sea and Fram Strait Arctic-Atlantic gateways. *Geochimica et Cosmochimica Acta*, *72*, 2854–2867. <https://doi.org/10.1016/j.gca.2008.04.008>
- Arsouze, T., Dutay, J.-C., Lacan, F., & Jeandel, C. (2009). Reconstructing the Nd oceanic cycle using a coupled dynamical—Biogeochemical model. *Biogeosciences Discussions*, *6*, 5549–5588. <https://doi.org/10.5194/bgd-6-5549-2009>
- Basak, C., Pahnke, K., Frank, M., Lamy, F., & Gersonde, R. (2015). Neodymium isotopic characterization of Ross Sea Bottom Water and its advection through the southern South Pacific. *Earth and Planetary Science Letters*, *419*, 211–221. <https://doi.org/10.1016/j.epsl.2015.03.011>
- Bau, M., & Dulski, P. (1996). Anthropogenic origin of positive gadolinium anomalies in river waters. *Earth and Planetary Science Letters*, *143*, 245–255. [https://doi.org/10.1016/0012-821X\(96\)00127-6](https://doi.org/10.1016/0012-821X(96)00127-6)
- Behrens, M. K., Muratli, J., Pradoux, C., Wu, Y., Böning, P., Brumsack, H. J., et al. (2016). Rapid and precise analysis of rare earth elements in small volumes of seawater—Method and intercomparison. *Marine Chemistry*, *186*, 110–120. <https://doi.org/10.1016/j.marchem.2016.08.006>
- Behrens, M. K., Pahnke, K., Paffrath, R., Schnetger, B., & Brumsack, H. J. (2018). Rare earth element distributions in the West Pacific: Trace element sources and conservative vs. non-conservative behavior. *Earth and Planetary Science Letters*, *486*, 166–177. <https://doi.org/10.1016/j.epsl.2018.01.016>
- Behrens, M. K., Pahnke, K., Schnetger, B., & Brumsack, H. J. (2018). Sources and processes affecting the distribution of dissolved Nd isotopes and concentrations in the West Pacific. *Geochimica et Cosmochimica Acta*, *222*, 508–534. <https://doi.org/10.1016/j.gca.2017.11.008>
- Bertram, C. J., & Elderfield, H. (1993). The geochemical balance of the rare earth elements and neodymium isotopes in the oceans. *Geochimica et Cosmochimica Acta*, *57*, 1957–1986. [https://doi.org/10.1016/0016-7037\(93\)90087-D](https://doi.org/10.1016/0016-7037(93)90087-D)
- Björk, G., Jakobsson, M., Rudels, B., Swift, J. H., Anderson, L., Darby, D. A., et al. (2007). Bathymetry and deep-water exchange across the central Lomonosov Ridge at 88–89°N. *Deep-Sea Research Part I*, *54*, 1197–1208. <https://doi.org/10.1016/j.dsr.2007.05.010>
- Byrne, R. H., & Kim, K.-H. (1990). Rare earth element scavenging in seawater. *Geochimica et Cosmochimica Acta*, *54*, 2645–2656. [https://doi.org/10.1007/s13398-014-0173-7.210.1016/0016-7037\(90\)90002-3](https://doi.org/10.1007/s13398-014-0173-7.210.1016/0016-7037(90)90002-3)
- Casacuberta, N., Christl, M., Vockenhuber, C., Wefing, A. M., Wacker, L., Masqué, P., et al. (2018). Tracing the three Atlantic branches entering the Arctic Ocean with ^{129}I and ^{236}U . *Journal of Geophysical Research: Oceans*, *123*, 6909–6921. <https://doi.org/10.1029/2018JC014168>
- Charette, M. A., Kipp, L. E., Jensen, L. T., Dabrowski, J. S., Whitmore, L. M., Fitzsimmons, J. N., et al. (2020). The transpolar drift as a source of riverine and shelf-derived trace elements to the central Arctic Ocean. *Journal of Geophysical Research: Oceans*, *125*. <https://doi.org/10.1029/2019jc015920>
- Chavagnac, V., Saleban Ali, H., Jeandel, C., Leleu, T., Destrienneville, C., Castillo, A., et al. (2018). Sulfate minerals control dissolved rare earth element flux and Nd isotope signature of buoyant hydrothermal plume (EMSO-Azores, 37°N Mid-Atlantic Ridge). *Chemical Geology*, *499*, 111–125. <https://doi.org/10.1016/j.chemgeo.2018.09.021>
- Cutter, G., Casciotti, K., Croot, P., Geibert, W., Heimbürger, L.-E., Lohan, M., et al. (2017). *Sampling and sample-handling protocols for GEOTRACES cruises*. GEOTRACES Cookbook. Retrieved from <http://www.geotraces.org/images/stories/documents/intercalibration/Cookbook.pdf>
- Dahlqvist, R., Andersson, P. S., & Porcelli, D. (2007). Nd isotopes in Bering Strait and Chukchi Sea water. *Geochimica et Cosmochimica Acta*, *71*, A196.
- Dymond, J., Collier, R., McManus, J., Honjo, S., & Manganini, S. (1997). Can the aluminum and titanium contents of ocean sediments be used to determine the paleoproductivity of the oceans? *Paleoceanography*, *12*, 586–593. <https://doi.org/10.1029/97PA01135>
- Edmonds, H. N., Michael, P. J., Baker, E. T., Connelly, D. P., Snow, J. E., Langmuir, C. H., et al. (2003). Discovery of abundant hydrothermal venting on the ultraslow-spreading Gakkel ridge in the Arctic Ocean. *Nature*, *421*, 252–256. <https://doi.org/10.1038/nature01319.1>
- Elderfield, H. (1988). The oceanic chemistry of rare-earth elements. *Philosophical Transactions of the Royal Society of London, Series A*, *325*, 105–126. <https://doi.org/10.1098/rsta.1988.0046>
- Eliseeva, S. V., & Bünzli, J. C. G. (2011). Rare earths: Jewels for functional materials of the future. *New Journal of Chemistry*, *35*, 1165–1176. <https://doi.org/10.1039/c0nj00969e>
- Fernández-Méndez, M., Katlein, C., Rabe, B., Nicolaus, M., Peeken, I., Bakker, K., et al. (2015). Photosynthetic production in the central Arctic Ocean during the record sea-ice minimum in 2012. *Biogeosciences*, *12*, 3525–3549. <https://doi.org/10.5194/bg-12-3525-2015>
- Fröllje, H., Pahnke, K., Schnetger, B., Brumsack, H. J., Dulai, H., & Fitzsimmons, J. N. (2016). Hawaiian imprint on dissolved Nd and Ra isotopes and rare earth elements in the central North Pacific: Local survey and seasonal variability. *Geochimica et Cosmochimica Acta*, *189*, 110–131. <https://doi.org/10.1016/j.gca.2016.06.001>
- García-Solsona, E., Jeandel, C., Labatut, M., Lacan, F., Vance, D., Chavagnac, V., & Pradoux, C. (2014). Rare earth elements and Nd isotopes tracing water mass mixing and particle-seawater interactions in the SE Atlantic. *Geochimica et Cosmochimica Acta*, *125*, 351–372. <https://doi.org/10.1016/j.gca.2013.10.009>
- Gdaniec, S., Roy-Barman, M., Foliot, L., Thil, F., Dapigny, A., Burckel, P., et al. (2018). Thorium and protactinium isotopes as tracers of marine particle fluxes and deep water circulation in the Mediterranean Sea. *Marine Chemistry*, *199*, 12–23. <https://doi.org/10.1016/j.marchem.2017.12.002>
- Gdaniec, S., Roy-Barman, M., Levier, M., Valk, O., van der Loeff, M. R., Foliot, L., et al. (2020). ^{231}Pa and ^{230}Th in the Arctic Ocean: Implications for boundary scavenging and ^{231}Pa – ^{230}Th fractionation in the Eurasian Basin. *Chemical Geology*, *532*, 119380. <https://doi.org/10.1016/j.chemgeo.2019.119380>
- German, C., Klinkhammer, G. P., Edmond, J. M., Mitra, A., & Elderfield, H. (1990). Hydrothermal scavenging of rare earth elements in the ocean. *Nature*, *346*, 818–822. [https://doi.org/10.1016/0021-9797\(80\)90501-9.10.1038/345516a0](https://doi.org/10.1016/0021-9797(80)90501-9.10.1038/345516a0)
- Grenier, M., François, R., Soon, M., Rutgers van der Loeff, M., Yu, X., Valk, O., et al. (2019). Circulation and particle scavenging in the Amerasian Basin of the Arctic Ocean over the last three decades inferred from the water column distribution of geochemical tracers. *Journal of Geophysical Research: Oceans*, *124*, 9338–9363. <https://doi.org/10.1029/2019JC015265>
- Grenier, M., Jeandel, C., Lacan, F., Vance, D., Venchiarutti, C., Cros, A., & Cravatte, S. (2013). From the subtropics to the central equatorial Pacific Ocean: Neodymium isotopic composition and rare earth element concentration variations. *Journal of Geophysical Research: Oceans*, *118*, 592–618. <https://doi.org/10.1029/2012JC008239>
- Hayes, C. T., Anderson, R. F., Fleisher, M. Q., Vivancos, S. M., Lam, P. J., Ohnemus, D. C., et al. (2015). Intensity of Th and Pa scavenging partitioned by particle chemistry in the North Atlantic Ocean. *Marine Chemistry*, *170*, 49–60. <https://doi.org/10.1016/j.marchem.2015.01.006>

- IPCC. (2014). *Climate change 2014: Synthesis report* (p. 151). Contribution of Working Groups I, II and III to the Fifth Assessment Report of the Intergovernmental Panel on Climate Change [Core Writing Team], IPCC.
- Jacobsen, S. B., & Wasserburg, G. J. (1980). Sm-Nd evolution of chondrites. *Earth and Planetary Science Letters*, 50, 139–155. [https://doi.org/10.1016/0012-821X\(80\)90125-9](https://doi.org/10.1016/0012-821X(80)90125-9)
- Jeandel, C. (1993). Concentration and isotopic composition of Nd in the South Atlantic Ocean. *Earth and Planetary Science Letters*, 117, 581–591. [https://doi.org/10.1016/0012-821X\(93\)90104-H](https://doi.org/10.1016/0012-821X(93)90104-H)
- Jeandel, C., Bishop, K. L., & Zindler, A. (1995). Exchange of neodymium and its isotopes between seawater and small and large particles in the Sargasso Sea. *Geochimica et Cosmochimica Acta*, 59, 535–547. [https://doi.org/10.1016/0016-7037\(94\)00367-u](https://doi.org/10.1016/0016-7037(94)00367-u)
- Jeandel, C., Delattre, H., Grenier, M., Pradoux, C., & Lacan, F. (2013). Rare earth element concentrations and Nd isotopes in the Southeast Pacific Ocean. *Geochemistry, Geophysics, Geosystems*, 14, 328–341. <https://doi.org/10.1029/2012GC004309>
- Jeandel, C., Thouron, D., & Fieux, M. (1998). Concentrations and isotopic compositions of neodymium in the eastern Indian Ocean and Indonesian straits. *Geochimica et Cosmochimica Acta*, 62, 2597–2607. [https://doi.org/10.1017/S002221510014808X10.1016/S0016-7037\(98\)00169-0](https://doi.org/10.1017/S002221510014808X10.1016/S0016-7037(98)00169-0)
- Jones, E. P., Rudels, B., & Anderson, L. G. (1995). Deep waters of the Arctic Ocean: Origins and circulation. *Deep-Sea Research Part I*, 42, 737–760. [https://doi.org/10.1016/0967-0637\(95\)00013-V](https://doi.org/10.1016/0967-0637(95)00013-V)
- Klinkhammer, G. P., Elderfield, H., & Hudson, A. (1983). Rare earth elements in seawater near hydrothermal vents. *Nature*, 305, 185–188. <https://doi.org/10.1038/305185a0>
- Klunder, M. B., Laan, P., Middag, R., de Baar, H. J. W., & Bakker, K. (2012). Dissolved iron in the Arctic Ocean: Important role of hydrothermal sources, shelf input and scavenging removal. *Journal of Geophysical Research*, 117. <https://doi.org/10.1029/2011JC007135>
- Kulaksiz, S., & Bau, M. (2007). Contrasting behaviour of anthropogenic gadolinium and natural rare earth elements in estuaries and the gadolinium input into the North Sea. *Earth and Planetary Science Letters*, 260, 361–371. <https://doi.org/10.1016/j.epsl.2007.06.016>
- Lacan, F., & Jeandel, C. (2001). Tracing Papua New Guinea imprint on the central Equatorial Pacific Ocean using neodymium isotopic compositions and rare earth element patterns. *Earth and Planetary Science Letters*, 186, 497–512. [https://doi.org/10.1016/S0012-821X\(01\)00263-1](https://doi.org/10.1016/S0012-821X(01)00263-1)
- Lacan, F., & Jeandel, C. (2005). Neodymium isotopes as a new tool for quantifying exchange fluxes at the continent-ocean interface. *Earth and Planetary Science Letters*, 232, 245–257. <https://doi.org/10.1016/j.epsl.2005.01.004>
- Lagarde, M., Lemaitre, N., Planquette, H., Grenier, M., Belhadj, M., Lherminier, P., & Jeandel, C. (2020). Particulate Rare Earth Element behavior in the North Atlantic (GEOVIDE cruise). *Biogeosciences Discussions*, 17, 5539–5561. <https://doi.org/10.5194/bg-2019-46210.5194/bg-17-5539-2020>
- Lam, P. J., & Marchal, O. (2015). Insights into particle cycling from thorium and particle data. *Annual Review of Marine Science*, 7, 159–184. <https://doi.org/10.1146/annurev-marine-010814-015623>
- Lam, P. J., Ohnemus, D. C., & Auro, M. E. (2015). Size-fractionated major particle composition and concentrations from the US GEOTRACES North Atlantic Zonal Transect. *Deep-Sea Research Part II*, 116, 303–320. <https://doi.org/10.1016/j.dsr2.2014.11.020>
- Lambelet, M., van de Flierdt, T., Crocket, K., Rehkämper, M., Kreissig, K., Coles, B., et al. (2016). Neodymium isotopic composition and concentration in the western North Atlantic Ocean: Results from the GEOTRACES GA02 section. *Geochimica et Cosmochimica Acta*, 177, 1–29. <https://doi.org/10.1016/j.gca.2015.12.019>
- Laukert, G., Frank, M., Bauch, D., Hathorne, E. C., Rabe, B., von Appen, W. J., et al. (2017). Ocean circulation and freshwater pathways in the Arctic Mediterranean based on a combined Nd isotope, REE and oxygen isotope section across Fram Strait. *Geochimica et Cosmochimica Acta*, 202, 285–309. <https://doi.org/10.1016/j.gca.2016.12.028>
- Laukert, G., Makhotin, M., Petrova, M. V., Frank, M., Hathorne, E. C., Bauch, D., et al. (2019). Water mass transformation in the Barents Sea inferred from radiogenic neodymium isotopes, rare earth elements and stable oxygen isotopes. *Chemical Geology*, 511, 416–430. <https://doi.org/10.1016/j.chemgeo.2018.10.002>
- Liguori, B. T. P., Ehlert, C., & Pahnke, K. (2020). The influence of water mass mixing and particle dissolution on the silicon cycle in the central Arctic Ocean. *Frontiers in Marine Science*, 7, 1–16. <https://doi.org/10.3389/fmars.2020.00202>
- Macdonald, R. W., Carmack, E. C., & Wallace, D. W. R. (1993). Tritium and radiocarbon dating of Canada basin deep waters. *Science*, 259, 103–104. <https://doi.org/10.1126/science.259.5091.103>
- Martin, E. E., Blair, S. W., Kamenov, G. D., Scher, H. D., Bourbon, E., Basak, C., & Newkirk, D. N. (2010). Extraction of Nd isotopes from bulk deep sea sediments for paleoceanographic studies on Cenozoic time scales. *Chemical Geology*, 269, 414–431. <https://doi.org/10.1016/j.chemgeo.2009.10.016>
- Michael, P. J., Langmuir, C. H., Dick, H. J. B., Snow, J. E., Goldstein, S. L., Graham, D. W., et al. (2003). Magmatic and amagmatic seafloor generation at the ultraslow-spreading Gakkel ridge, Arctic Ocean. *Nature*, 423, 956–961. <https://doi.org/10.1038/nature01704>
- Midttun, L. (1985). Formation of dense bottom water in the Barents Sea. *Deep-Sea Research Part A*, 32, 1233–1241. [https://doi.org/10.1016/0198-0149\(85\)90006-8](https://doi.org/10.1016/0198-0149(85)90006-8)
- Mitra, A., Elderfield, H., & Greaves, M. J. (1994). Rare earth elements in submarine hydrothermal fluids and plumes from the Mid-Atlantic Ridge. *Marine Chemistry*, 46, 217–235. [https://doi.org/10.1016/0304-4203\(94\)90079-5](https://doi.org/10.1016/0304-4203(94)90079-5)
- Molina-Kescher, M., Frank, M., & Hathorne, E. (2014). South Pacific dissolved Nd isotope compositions and rare earth element distributions: Water mass mixing versus biogeochemical cycling. *Geochimica et Cosmochimica Acta*, 127, 171–189. <https://doi.org/10.1016/j.gca.2013.11.038>
- Naumov, A. (2008). Review of the world market of rare-earth metals. *Metallurgy of rare and noble metals*, 49, 14–22. <https://doi.org/10.3103/S1067821208010045>
- O’Nions, R. K., Hamilton, P. J., & Evensen, N. M. (1977). Variations in $^{143}\text{Nd}/^{144}\text{Nd}$ and $^{87}\text{Sr}/^{86}\text{Sr}$ ratios in oceanic basalts. *Earth and Planetary Science Letters*, 34, 13–22. <https://doi.org/10.4324/9781315413617>
- Osborne, A. H., Haley, B. A., Hathorne, E. C., Plancherel, Y., & Frank, M. (2014). Rare earth element distribution in Caribbean seawater: Continental inputs versus lateral transport of distinct REE compositions in subsurface water masses. *Marine Chemistry*, 177, 172–183. <https://doi.org/10.1016/j.marchem.2015.03.013>
- Paffrath, R., Laukert, G., Bauch, D., Rutgers van der Loeff, M., & Pahnke, K. (2021). Separating individual contributions of major Siberian rivers in the Transpolar Drift of the Arctic Ocean. *Scientific Reports*, 11, 8216. <https://doi.org/10.1038/s41598-021-86948-y>
- Paffrath, R., Pahnke, K., Behrens, M. K., Reckhardt, A., Ehlert, C., Schnetger, B., & Brumsack, H.-J. (2020). Rare earth element behavior in a sandy subterranean estuary of the southern North Sea. *Frontiers in Marine Science*, 7, 1–18. <https://doi.org/10.3389/fmars.2020.00424>
- Paffrath, R., Pahnke, K., Böning, P., Rutgers van der Loeff, M. M., Valk, O., Gdaniec, S., & Planquette, H. (2021a). Dissolved rare earth element concentrations and neodymium isotope compositions in the central Arctic Ocean during FS Polarstern PS94 (GEOTRACES GN04). PANGAEA. <https://doi.org/10.1594/PANGAEA.933493>

- Paffrath, R., Pahnke, K., Böning, P., Rutgers van der Loeff, M. M., Valk, O., Gdaniec, S., & Planquette, H. (2021b). *Particulate rare earth element concentrations and neodymium isotope compositions in the central Arctic Ocean during FS Polarstern PS94 (GEOTRACES GN04)*. PANGAEA. <https://doi.org/10.1594/PANGAEA.933484>
- Pearce, C. R., Jones, M. T., Oelkers, E. H., Pradoux, C., & Jeandel, C. (2013). The effect of particulate dissolution on the neodymium (Nd) isotope and Rare Earth Element (REE) composition of seawater. *Earth and Planetary Science Letters*, 369–370, 138–147. <https://doi.org/10.1016/j.epsl.2013.03.023>
- Pedreira, R. M. A., Pahnke, K., Böning, P., & Hatje, V. (2018). Tracking hospital effluent-derived gadolinium in Atlantic coastal waters off Brazil. *Water Research*, 145, 62–72. <https://doi.org/10.1016/j.watres.2018.08.005>
- Pin, C., & Zalduendi, J. (1997). Sequential separation of light rare-earth elements, thorium and uranium by miniaturized extraction chromatography: Application to isotopic analyses of silicate rocks. *Analytica Chimica Acta*, 339, 79–89. [https://doi.org/10.1016/S0003-2670\(96\)00499-0](https://doi.org/10.1016/S0003-2670(96)00499-0)
- Planquette, H., & Sherrell, R. M. (2012). Sampling for particulate trace element determination using water sampling bottles: Methodology and comparison to in situ pumps. *Limnology and Oceanography: Methods*, 10, 367–388. <https://doi.org/10.4319/lom.2012.10.367>
- Porcelli, D., Andersson, P. S., Baskaran, M., Frank, M., Björk, G., & Semiletov, I. (2009). The distribution of neodymium isotopes in Arctic Ocean basins. *Geochimica et Cosmochimica Acta*, 73, 2645–2659. <https://doi.org/10.1016/j.gca.2008.11.046>
- Rabe, B., Schauer, U., Ober, S., Horn, M., Hoppmann, M., Korhonen, M., et al. (2016). *Physical oceanography measured on water bottle samples during POLARSTERN cruise PS94 (ARK-XXIX/3)*. Alfred Wegener Institute, Helmholtz Center for Polar and Marine Research. <https://doi.org/10.1594/PANGAEA.859559>
- Rijkenberg, M. J. A., Slagter, H. A., Rutgers van der Loeff, M., van Ooijen, J., & Gerringa, L. J. A. (2018). Dissolved Fe in the deep and upper Arctic Ocean with a focus on Fe limitation in the Nansen Basin. *Frontiers in Marine Science*, 5, 1–14. <https://doi.org/10.3389/fmars.2018.00088>
- Roberts, N. L., Piotrowski, A. M., Elderfield, H., Eglinton, T. I., & Lomas, M. W. (2012). Rare earth element association with foraminifera. *Geochimica et Cosmochimica Acta*, 94, 57–71. <https://doi.org/10.1016/j.gca.2012.07.009>
- Rousseau, T. C. C., Sonke, J. E., Chmieleff, J., van Beek, P., Souhaut, M., Boaventura, G., et al. (2015). Rapid neodymium release to marine waters from lithogenic sediments in the Amazon estuary. *Nature Communications*, 6, 1–8. <https://doi.org/10.1038/ncomms8592>
- Rudels, B. (2009). Arctic Ocean circulation. In *Encyclopedia of ocean sciences* (pp. 211–225). <https://doi.org/10.1016/B978-012374473-9.00601-9>
- Rudels, B., Anderson, L., Eriksson, P., Fahrback, E., Jakobsson, M., Jones, E. P., et al. (2012). Observations in the Ocean. In P. Lemke, & H.-W. Jacobi (Eds.), *Arctic climate change: The ACSYS decade and beyond* (Vol. 43, pp. 117–198). https://doi.org/10.1007/978-94-007-2027-510.1007/978-94-007-2027-5_4
- Rudels, B., Korhonen, M., Schauer, U., Pisarev, S., Rabe, B., & Wisotzki, A. (2015). Circulation and transformation of Atlantic water in the Eurasian Basin and the contribution of the Fram Strait inflow branch to the Arctic Ocean heat budget. *Progress in Oceanography*, 132, 128–152. <https://doi.org/10.1016/j.pocean.2014.04.003>
- Rudnick, R. L., & Gao, S. (2003). Composition of the continental crust. In H. D. Holland, & K. K. Turekian (Eds.), *Treatise on geochemistry* (pp. 1–64). Elsevier. <https://doi.org/10.1016/B0-08-043751-6/03016-4>
- Schijf, J., Christenson, E. A., & Byrne, R. H. (2015). YREE scavenging in seawater: A new look at an old model. *Marine Chemistry*, 177, 460–471. <https://doi.org/10.1016/j.marchem.2015.06.010>
- Schlitzer, R. (2018). *Ocean data view*. Retrieved from <https://odv.awi.de>
- Schlosser, P., Kromer, B., Ostlund, G., Ekwurzel, B., Bonisch, G., Loosli, H. H., & Purtschert, R. (1994). On the ¹⁴C and ³⁹Ar distribution in the Central Arctic Ocean: Implications for deep water formation. *Radiocarbon*, 36, 327–343. <https://doi.org/10.1017/s003382220001451x>
- Schmitt, W. (2007). *Application of the Sm-Nd isotope system to the late quaternary paleoceanography of the Yermak Plateau (Arctic Ocean)* (PhD thesis). Ludwig-Maximilians-University Munich, Faculty of Geosciences.
- Shabani, M. B., Akagi, T., & Masuda, A. (1992). Preconcentration of trace rare-earth elements in seawater by complexation with Bis(2-ethylhexyl) hydrogen phosphate and 2-ethylhexyl dihydrogen phosphate adsorbed on a C18 cartridge and determination by inductively coupled plasma mass spectrometry. *Analytical Chemistry*, 64, 737–743. <https://doi.org/10.1021/ac00031a008>
- Sholkovitz, E. R. (1995). The aquatic chemistry of rare earth elements in rivers and estuaries. *Aquatic Geochemistry*, 1, 1–34. <https://doi.org/10.1007/bf01025229>
- Sholkovitz, E. R., Landing, W. M., & Lewis, B. L. (1994). Ocean particle chemistry: The fractionation of rare earth elements between suspended particles and seawater. *Geochimica et Cosmochimica Acta*, 58, 1567–1579. [https://doi.org/10.1016/0016-7037\(94\)90559-2](https://doi.org/10.1016/0016-7037(94)90559-2)
- Siddall, M., Khatiwala, S., van de Flierdt, T., Jones, K., Goldstein, S. L., Hemming, S., & Anderson, R. F. (2008). Toward explaining the Nd paradox using reversible scavenging in an ocean general circulation model. *Earth and Planetary Science Letters*, 274, 448–461. <https://doi.org/10.1016/j.epsl.2008.07.044>
- Slagter, H. A., Reader, H. E., Rijkenberg, M. J. A., Rutgers van der Loeff, M., de Baar, H. J. W., & Gerringa, L. J. A. (2017). Organic Fe speciation in the Eurasian Basins of the Arctic Ocean and its relation to terrestrial DOM. *Marine Chemistry*, 197, 11–25. <https://doi.org/10.1016/j.marchem.2017.10.005>
- Smethie, W. M., Newton, R., Schlosser, P., & Pasqualini, A. (2019). *Relic water in the deep Arctic Ocean*. Goldschmidt Abstract.
- Stichel, T., Hartman, A. E., Duggan, B., Goldstein, S. L., Scher, H., & Pahnke, K. (2015). Separating biogeochemical cycling of neodymium from water mass mixing in the Eastern North Atlantic. *Earth and Planetary Science Letters*, 412, 245–260. <https://doi.org/10.1016/j.epsl.2014.12.008>
- Stichel, T., Pahnke, K., Duggan, B., Goldstein, S. L., Hartman, A. E., Paffrath, R., & Scher, H. D. (2018). TAG plume: Revisiting the hydrothermal neodymium contribution to seawater. *Frontiers in Marine Science*, 5, 1–11. <https://doi.org/10.3389/fmars.2018.00096>
- Stranne, C., Sohn, R. A., Liljebladh, B., & Nakamura, K. I. (2010). Analysis and modeling of hydrothermal plume data acquired from the 85°E segment of the Gakkel Ridge. *Journal of Geophysical Research*, 115, 1–17. <https://doi.org/10.1029/2009JC005776>
- Swift, J. H., Takahashi, T., & Livingston, H. D. (1983). Contribution of the Greenland and Barents Seas to the deep water of the Arctic Ocean. *Journal of Geophysical Research*, 88, 5981–5986. <https://doi.org/10.1029/JC088iC10p05981>
- Tachikawa, K., Athias, V., & Jeandel, C. (2003). Neodymium budget in the modern ocean and paleo-oceanographic implications. *Journal of Geophysical Research*, 108, 3254. <https://doi.org/10.1029/1999JC000285>
- Tachikawa, K., Jeandel, C., & Dupré, B. (1997). Distribution of rare earth elements and neodymium isotopes in settling particulate material of the tropical Atlantic Ocean (EUMELI site). *Deep-Sea Research Part I Oceanographic Research Papers*, 44, 1769–1792. [https://doi.org/10.1016/S0967-0637\(97\)00057-5](https://doi.org/10.1016/S0967-0637(97)00057-5)

- Tachikawa, K., Jeandel, C., Vangriesheim, A., & Dupré, B. (1999). Distribution of rare earth elements and neodymium isotopes in suspended particles of the tropical Atlantic Ocean (EUMELI site). *Deep-Sea Research Part I Oceanographic Research Papers*, 46, 733–755. [https://doi.org/10.1016/S0967-0637\(98\)00089-2](https://doi.org/10.1016/S0967-0637(98)00089-2)
- Tanaka, T., Togashi, S., Kamioka, H., Amakawa, H., Kagami, H., Hamamoto, T., et al. (2000). JNdi-1: A neodymium isotopic reference in consistency with LaJolla neodymium. *Chemical Geology*, 168, 279–281. [https://doi.org/10.1016/S0009-2541\(00\)00198-4](https://doi.org/10.1016/S0009-2541(00)00198-4)
- Timmermans, M.-L., Garrett, C., & Carmack, E. (2003). The thermohaline structure and evolution of the deep waters in the Canada Basin, Arctic Ocean. *Deep-Sea Research Part I*, 50, 1305–1321. [https://doi.org/10.1016/S0967-0637\(03\)00125-0](https://doi.org/10.1016/S0967-0637(03)00125-0)
- Timmermans, M.-L., Winsor, P., & Whitehead, J. A. (2005). Deep-water flow over the Lomonosov Ridge in the Arctic Ocean. *Journal of Physical Oceanography*, 35, 1489–1493. <https://doi.org/10.1175/JPO2765.1>
- Valk, O., Rutgers van der Loeff, M. M., Geibert, W., Gdaniec, S., Rijkenberg, M. J. A., Moran, S. B., et al. (2018). Importance of hydrothermal vents in scavenging removal of ²³⁰Th in the Nansen Basin. *Geophysical Research Letters*, 45, 10539–10548. <https://doi.org/10.1029/2018GL079829>
- Vance, D., & Thirlwall, M. (2002). An assessment of mass discrimination in MC-ICPMS using Nd isotopes. *Chemical Geology*, 185, 227–240. [https://doi.org/10.1016/S0009-2541\(01\)00402-8](https://doi.org/10.1016/S0009-2541(01)00402-8)
- van de Fliert, T., Griffiths, A. M., Lambelet, M., Little, S. H., Stichel, T., & Wilson, D. J. (2016). Neodymium in the oceans: A global database, a regional comparison and implications for palaeoceanographic research. *Philosophical Transactions of the Royal Society A: Mathematical, Physical and Engineering Sciences*, 374. <https://doi.org/10.1098/rsta.2015.0293>
- van de Fliert, T., Pahnke, K., Amakawa, H., Andersson, P., Basak, C., Coles, B., et al. (2012). GEOTRACES intercalibration of neodymium isotopes and rare earth element concentrations in seawater and suspended particles. Part 1: Reproducibility of results for the international intercomparison. *Limnology and Oceanography: Methods*, 10, 234–251. <https://doi.org/10.4319/lom.2012.10.234>
- van Ooijen, J. C., Rijkenberg, M. J. A., Gerringa, L. J. A., Rabe, B., & Rutgers van der Loeff, M. M. (2016). *Inorganic nutrients measured on water bottle samples during POLARSTERN cruise PS94 (ARK-XXIX/3)*. Royal Netherlands Institute for Sea Research. <https://doi.pangaea.de/10.1594/PANGAEA.868396>
- Voncken, J. H. L. (2016). *The rare earth elements: An introduction*. Springer Nature. <https://doi.org/10.1007/978-3-319-26809-5>
- Westerlund, S., & Öhman, P. (1992). Rare earth elements in the Arctic Ocean. *Deep-Sea Research Part A*, 39, 1613–1626. [https://doi.org/10.1016/0198-0149\(92\)90051-T](https://doi.org/10.1016/0198-0149(92)90051-T)
- Yang, J., & Haley, B. A. (2016). The profile of the rare earth elements in the Canada Basin, Arctic Ocean. *Geochemistry, Geophysics, Geosystems*, 17, 3241–3253. <https://doi.org/10.1002/2016GC006412>
- Zheng, X. Y., Plancherel, Y., Saito, M. A., Scott, P. M., & Henderson, G. M. (2016). Rare earth elements (REEs) in the tropical South Atlantic and quantitative deconvolution of their non-conservative behavior. *Geochimica et Cosmochimica Acta*, 177, 217–237. <https://doi.org/10.1016/j.gca.2016.01.018>
- Zimmermann, B., Porcelli, D., Frank, M., Andersson, P. S., Baskaran, M., Lee, D. C., & Halliday, A. N. (2009). Hafnium isotopes in Arctic Ocean water. *Geochimica et Cosmochimica Acta*, 73, 3218–3233. <https://doi.org/10.1016/j.gca.2009.02.028>